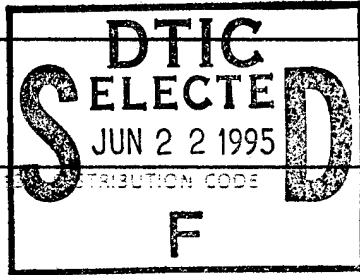


REPORT DOCUMENTATION PAGE			Form Approved OMB No. 0704-0188	
<small>Public reporting burden for this collection of information is estimated to average 1 hour per response, including the time for reviewing instructions, searching existing data sources, gathering and maintaining the data needed, and completing and reviewing this collection of information. Send comments regarding this burden estimate or any other aspect of this collection of information, including suggestions for reducing this burden, to: Washington Headquarters Services, Directorate for Information Operations and Reports, 1215 Jefferson Davis Highway, Suite 1204, Arlington, VA 22202-4302, and to the Office of Management and Budget, Paperwork Reduction Project (0704-0188), Washington, DC 20503.</small>				
1. AGENCY USE ONLY (Leave blank)		2. REPORT DATE		3. REPORT TYPE AND DATES COVERED FINAL/01 OCT 91 TO 31 MAR 95
4. TITLE AND SUBTITLE THE USE OF AIR FORCE CLOUD COVER DATA TO EVALUATE AND IMPROVE CLOUD FORECAST & PARAMETERIZATION IN MESOSCALE METEOROLOGY MODELS			5. FUNDING NUMBERS	
6. AUTHOR(S) CHRIS J. WALCEK			2310/CS F49620-92-J-0018	
7. PERFORMING ORGANIZATION NAME(S) AND ADDRESS(ES) ATMOSPHERIC SCIENCES RESEARCH CENTER STATE UNIVERSITY OF NEW YORK AT ALBANY 100 FULLER ROAD ALBANY, NY 12205			8. PERFORMING ORGANIZATION REPORT NUMBER AFOSR-TR-95-0426	
9. SPONSORING/MONITORING AGENCY NAME(S) AND ADDRESS(ES) AFOSR/NM 110 DUNCAN AVE, SUITE B115 BOLLING AFB DC 20332-0001			10. SPONSORING/MONITORING AGENCY REPORT NUMBER F49620-92-J-0018	
11. SUPPLEMENTARY NOTES				
12. DISTRIBUTION AVAILABILITY STATEMENT APPROVED FOR PUBLIC RELEASE: DISTRIBUTION IS UNLIMITED				
13. ABSTRACT (Maximum 200 words) Current methods of forecasting cloud cover within meteorology forecast models contain a high level of uncertainty. The primary goal of this research program was to reduce this uncertainty by utilizing satellite and surface-derived cloud observations together with standard meteorological measurements to evaluate and improve our ability to accurately diagnose and forecast cloud coverage. 19950619 010				
14. SUBJECT TERMS			15. NUMBER OF PAGES	
			16. PRICE CODE	
17. SECURITY CLASSIFICATION OF REPORT UNCLASSIFIED	18. SECURITY CLASSIFICATION OF THIS PAGE UNCLASSIFIED	19. SECURITY CLASSIFICATION OF ABSTRACT UNCLASSIFIED	20. LIMITATION OF ABSTRACT SAR(SAME AS REPORT)	

Final Technical Report

**The Use of Air Force Cloud Cover Data to Evaluate and Improve Cloud
Forecast & Parameterization in Mesoscale Meteorology Models**

1 October 1991 - 30 April 1995

Air Force Office of Scientific Research Grant # F49620-92-J0018

Accession For	
NTIS CRA&I	<input checked="" type="checkbox"/>
DTIC TAB	<input type="checkbox"/>
Unannounced	<input type="checkbox"/>
Justification	
By	
Distribution /	
Availability Codes	
Dist	Avail and/or Special
A-1	

Prepared for:

Major James Kroll, Program Manager
Air Force Office of Scientific Research
110 Duncan Ave., Suite B115
Bolling Air Force Base
Washington, D. C. 20332-0001

Prepared by:

Chris J. Walcek, Principal Investigator
Atmospheric Sciences Research Center
State University of New York at Albany
100 Fuller Rd.
Albany, NY 12205
voice phone (518) 442-3840
FAX (518) 442-9071
e-mail walcek@contrail.asrc.albany.edu

19 May 1995

Project Goals: Current methods of forecasting cloud cover within meteorology forecast models contain a high level of uncertainty. The primary goal of this research program was to reduce this uncertainty by utilizing satellite and surface-derived cloud observations together with standard meteorological measurements to evaluate and improve our ability to accurately diagnose and forecast cloud coverage.

1. Abstract of Research Findings

A major finding of this research effort was a determination of the **functional relationship between cloud cover and relative humidity**. Cloud cover in any atmospheric level decreases **exponentially** as the layer-averaged relative humidity falls below 100%. This study provides one of the few **observationally-derived** functional relationships for estimating cloud cover from relative humidity. Previous assumed relationships were based largely on ad hoc assumptions or extremely sparse observations, and thus varied widely: from simple “step function”, on/off formulations, to more elaborate linear or quadratic approximations. Nearly all previous cloud cover algorithms assume that mesoscale cloud cover disappeared when relative humidities fell below “critical relative humidities” in the 60-90% range. We found no observational support for this assumption, and our findings suggest that small cloud amounts occur at nearly **all** relative humidities. These results suggest that current meteorology and climate models probably underestimate the presence of clouds, especially at humidities below the “critical” humidities used by most models.

We also discovered that for the same relative humidities, convection tends to enhance cloud coverage in the upper troposphere, and decrease cloud coverage in the lower troposphere presumably due to the effects of cumulus-induced subsidence. We have developed an **innovative mass-flux convective parameterization** for calculating convective tendencies of heat and moisture to quantify the influence of convection on cloud cover. This work was initiated under sponsorship of this grant, and continues with support from an AASERT augmentation award and other granting agencies.

2. Project Summary

During this 42-month research effort, we have addressed the following topics:

- Derivation of functional relationship between cloud cover and relative humidity;
- Analysis of upper tropospheric relative humidity bias in a weather forecast model;
- Development and testing of alternate mass-flux convective parameterization;
- Begin simulations of a nonhydrostatic convective cloud model for testing convective parameterizations.

These subject areas will be briefly discussed in this technical report, and key figures summarizing research findings will be provided.

2.1 Cloud-cover & relative humidity: Most of our findings, the approach used, and fundamental functional relationships for calculating cloud cover are published in the journal *Monthly Weather Review*, included as an appendix supplement to this technical report. Vertical distributions of fractional cloud coverage derived from the U. S. Air Force 3DNEPH satellite, aircraft, and surface-based analysis were compared with related standard meteorological observations over the eastern U. S.. Cloud cover and related observations were interpolated onto the identical three-dimensional grid consisting of 15 tropospheric levels at various horizontal resolutions for five local noon periods during a springtime midlatitude cyclone. Mean fractional cloud coverage observed at various relative humidities and pressures were derived from these observations, and resolution-dependent algorithms for estimating cloud coverage from relative humidity are suggested. Despite a high degree of measurement uncertainty, it appears that cloud cover decreases exponentially as humidity falls below 100%, and relative to other layers in the troposphere, the layers 2.5 to 5 km above the surface contain the highest cloud amounts at the lowest relative humidities, with mean cloud amounts of 30% near 50% humidity at 650 mb.

Figure 1 best summarizes the discrepancies between previous cloud cover algorithms and what we find in this study. Many meteorological forecast models specify cloud amounts less than reported by these observations. When relative humidities are less than 90-95%, current

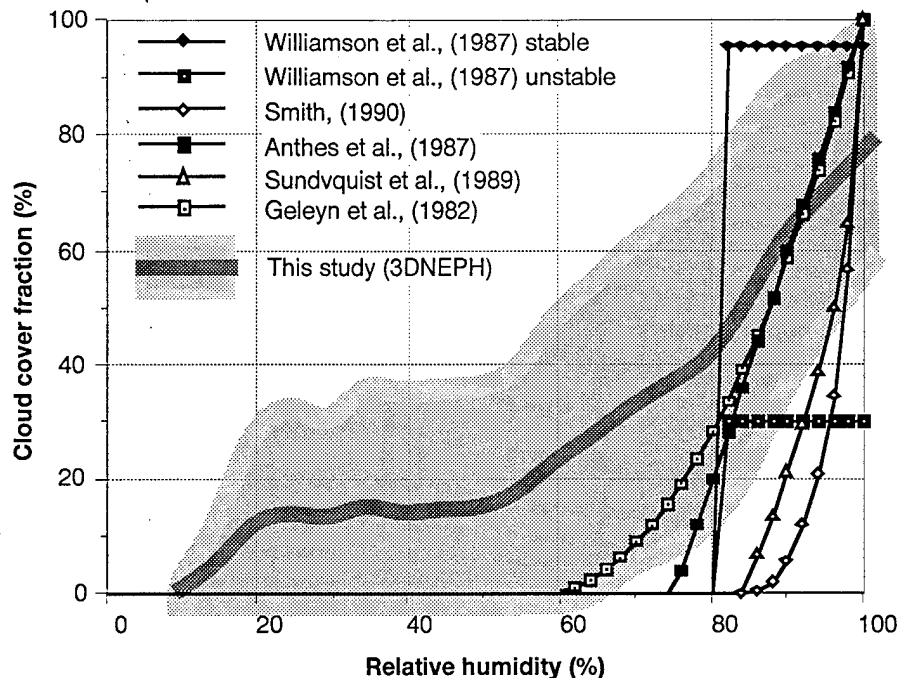


Figure 1: Fractional cloud coverage as a function of relative humidity at 800 mb according to various formulations used by meso- and global-scale atmospheric models. Shaded curve and area shows mean \pm standard deviation of 3DNEPH cloud cover at specified relative humidity during five noon periods during 20-24 April 1981.

meteorological models underpredict cloud coverage. At humidities close to saturation, current algorithms probably overestimate cloud coverage at many atmospheric levels. The functional relationships between cloud cover and relative humidity proposed in this study are probably more accurate than previous formulations, since they are based on a relatively large sample of simultaneous observations of both cloud cover and relative humidity.

The analysis used to generate Fig. 1 was repeated for all tropospheric levels, and contours of the average cloud cover at various pressures and relative humidities are shown in Fig 2. As shown in Figs. 1-2, cloud cover appears to decrease gradually in an approximately exponential fashion as relative humidity falls below 100%. Relative to other layers in the troposphere, the 800-600 mb layers contain the highest cloud amounts at the lowest relative humidities, with mean cloud amounts of 30% near 50% humidity at 650 mb. It should be noted that most existing cloud cover formulations specify totally clear skies at relative humidities below 50-80% at all tropospheric

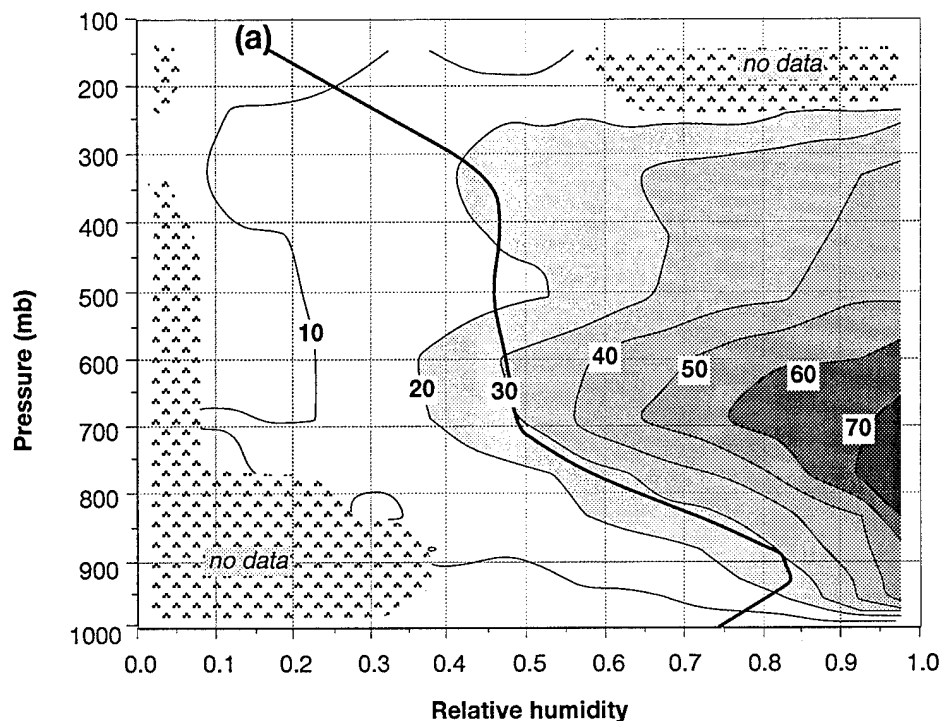


Figure 2: Mean cloud cover (%) at various pressures and relative humidities in the atmosphere during five noon periods during 20-24 April 1981 over the eastern U. S. . Curve shows mean relative humidity during same period.

layers, in stark contrast to the trends reported in Fig. 2, where up to 20% cloud cover is observed at relative humidities as low as 35%!

Based on our analysis, we suggest the following algorithm for calculating cloud cover (f) from relative humidity (Rh):

$$f = f_{100} \exp \left\{ \frac{Rh - 1}{1 - Rh_e} \right\} \quad (1)$$

where f_{100} is the cloud cover extrapolated to saturated ($Rh=100\%$) conditions, and $(1-Rh_e)$ is the humidity depression where cloud cover falls to $1/e$ (36.8%) of its coverage at $Rh=100\%$. Height and resolution-dependent algorithms empirically derived from the 3DNEPH are provided in Walcek (1994), attached as an appendix to this technical report.

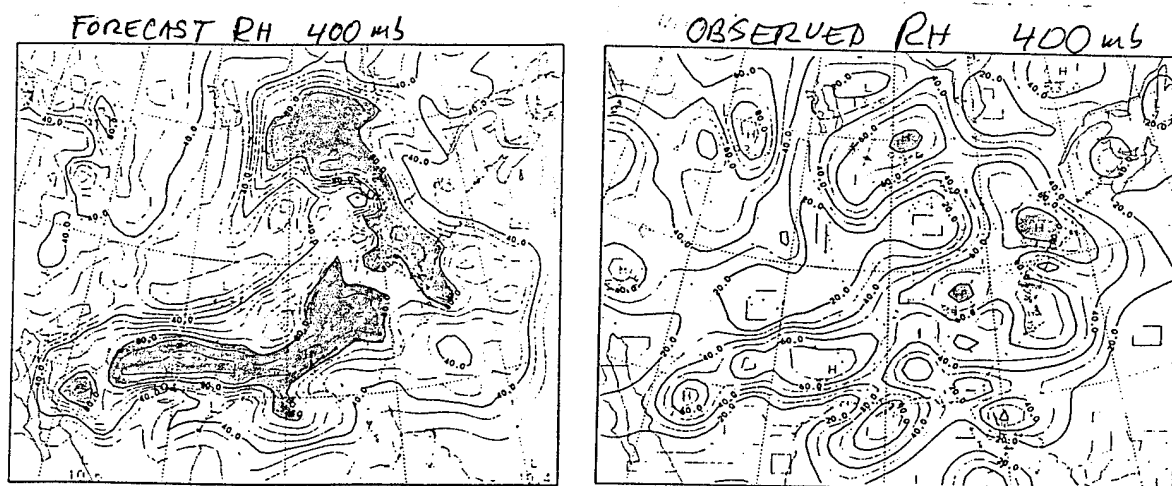


Figure 3: (left) 36-hour forecast and (right) verification observed relative humidity at 400 mb at 12 UT, 23 April 1981. MM4/NCAR forecast model initialized with observed humidities, winds, and temperatures 36 hours before time shown. Domain encompasses continental U. S.. shaded areas denote relative humidities greater than 80%.

2.2 Upper troposphere relative humidity bias: As described in Walcek (1994), we noted an apparent inconsistency between 3DNEPH cloud cover and model-interpolated relative humidity in the upper troposphere under dry, unstable conditions. At the same relative humidity, cloud cover was generally lower when convection was occurring in the drier regions of the upper troposphere relative to times when there was no convection. This result was non-intuitive, since convection should induce cloud formation, especially in the dry upper troposphere. We further investigated this problem by running the NCAR MM4 meteorology model in a purely forecast mode (rather than an observation-assimilation/interpolation mode), and compared model calculations with observations during one forecast period. Fig. 3 shows one comparison of relative humidity (with respect to liquid water) on the 400 mb surface forecast by MM4 compared with observations at the same time. The gray area on these figures denotes areas on the 400 mb surface with relative humidities greater than 80%. In a predictive mode, the NCAR Mesoscale meteorology model calculates excessive relative humidity in the upper troposphere along cold frontal, unstable regions. Discussions with other Air Force and University research groups reveal that this relative humidity bias is a long-standing problem for many regional and

global-scale meteorology models. Since the MM4 was used to "dynamically interpolate" the relative humidity observations in the Walcek (1994) study, we felt that there were some model-biases being introduced into the upper troposphere interpolation, especially when humidity observations are not very reliable. Since relative humidity is probably the most important parameter for specifying cloud coverage, any Rh error will introduce considerable uncertainty in cloud cover forecasts. We hypothesize that this relative humidity bias could be caused by two model attributes:

- An incorrect parameterization of moisture redistribution and removal by the convective-scale instabilities parameterized within the model;
- Unrealistic "numerical diffusion" of water vapor in regions of mean upward motion.

We suspect these two factors because a careful analysis of model-forecast humidity shows a bias only in conditionally unstable regions, which coincidentally occurs in conjunction with larger-scale upward motions in the atmosphere.

Numerical diffusion: Numerical diffusion occurs within grid-point models when advected or predicted variables have strong spatial gradients or fluctuations in the directions in which they are being advected. Water vapor always has a very strong vertical gradient in the atmosphere, since its vapor pressure is a strong function of temperature, and temperature decreases dramatically with height in the troposphere. To further study the source of excess moisture in the upper troposphere, we performed model forecasts using a version of MM4 that did not allow any convective-scale mixing. Within these simulations, only larger-scale advection and rainout of moisture affects water vapor fields in the troposphere. Model forecasts still contained the relative humidity bias in the upper troposphere under unstable conditions, suggesting that numerical diffusion could be occurring. If numerical diffusion were responsible for the bias, then increasing the vertical model resolution should alleviate this bias. We have run a version of the model using double the number of vertical layers, and still find excessive humidity in the upper

troposphere, suggesting that even higher vertical resolution may be required to remove numerical diffusion from model forecasts.

Convective mass flux model: In an attempt to investigate whether the convective processes are responsible for the relative humidity bias in unstable areas, we developed and tested an improved convective-scale vertical mixing parameterization for use in mesoscale meteorological models. The parameterization is being evaluated with observations of tropical convection gathered during the GATE field program in 1974. This convective mixing algorithm is based on a "detraining cloud-ensemble" description of buoyantly-driven cloud motions, and includes multi-stream cloud up- and down-drafts with somewhat more sophisticated microphysics than are currently incorporated into most cumulus parameterizations. This new cumulus parameterization calculates the heating and moistening tendencies due to buoyantly-induced convection within hydrostatic models of the atmosphere that cannot explicitly compute these effects. As shown in Fig. 4, initial predictions of convective-scale heating, moistening, and precipitation are very promising. Such an improved convective mixing algorithm should improve forecasts of water vapor in the upper troposphere, since convective-scale processes are the dominant mechanism for supplying and removing water vapor from the upper troposphere. As shown in Fig. 4, the dominant effect of tropical convection is to remove moisture and heat the upper troposphere. Therefore, intense convection should DRY the upper troposphere, and an underestimate of this drying effect could produce the relative humidity bias that we are seeing with the MM4 meteorology model. We have adopted previously-suggested closure assumptions within this new parameterization, but find evidence for a new closure: an approximately fixed fraction of the mass of any unstable layer in the atmosphere leaves that layer per hour. This closure assumption was suggested after careful analysis of the GATE observations that were used to evaluate this parameterization. As found in Walcek (1994), convection strongly influences cloud coverage, yet quantitative measures of the convective factors that influence cloud coverage are still lacking. This parameterization could ultimately provide measures of convective mass flux redistribution for use in cloud coverage algorithms. We are continuing to analyze the correlation between derived

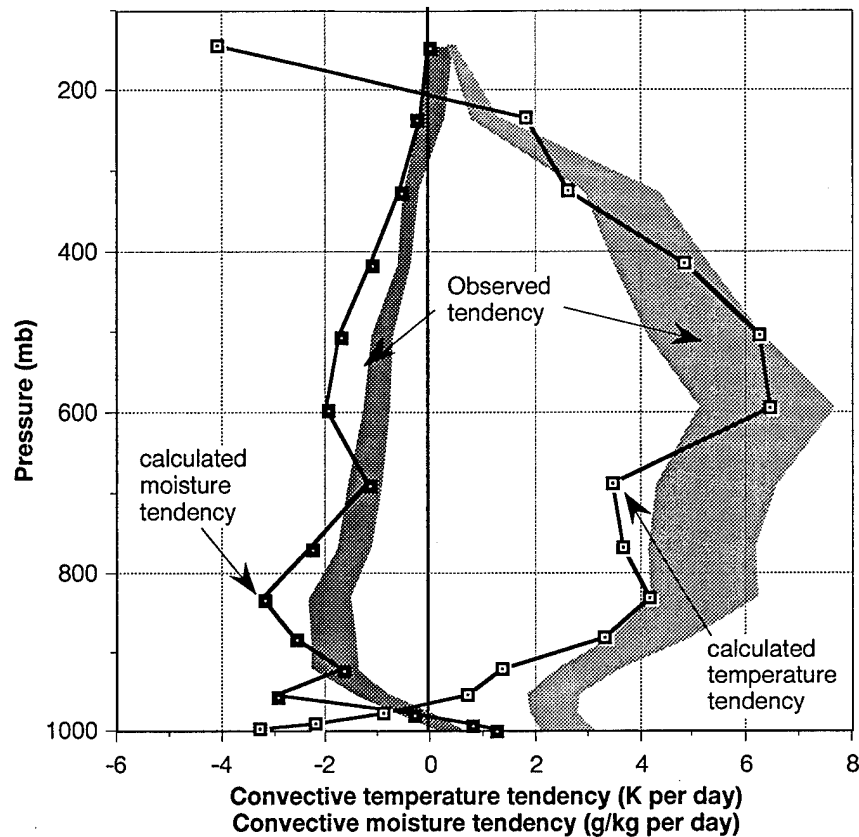


Figure 4: Comparison of calculated and observed temperature and moisture tendency due to convective effects during GATE (GARP Atlantic Tropical Experiment). Measurement made in the equatorial Atlantic during 1-18 September 1974. Calculations use measured atmospheric profiles within the convective parameterization developed during this project.

mass fluxes or other measures of convective intensity and the Air Force-archived 3DNEPH and RTNEPH cloud observations. This new convective parameterization could also provide more accurate relative humidity estimates in the upper troposphere, thus improving our ability to forecast cloud cover from more routinely-predicted relative humidity.

In addition to the time devoted by Dr. Walcek to this research effort, two research associates (Dr. Kesu Zhang and Dr. Hu Qi), a post-doctoral professional (Dr. Nenad Aleksic) and a graduate student (Mr. Bob Iacovazzi) have contributed to various technical aspects of this project.

3. Continuing research

One graduate student (Mr. Bob Iacovazzi) has been funded with an AASERT augmentation award to be trained and contribute to the objectives of this project. The augmentation moneys continue for an additional year (until June 1996), during which he will further develop and test a convective parameterization using 2- and 3-dimensional nonhydrostatic cloud-resolving models of convection. Mr. Iacovazzi will continue to analyze and improve methods of estimating cloud cover from related meteorology parameters. In particular, his emphasis will be to further investigate the relationship between cloud cover and convective activity as parameterized using our new convective mixing algorithm. We will begin including methods of assessing cloud cover from convective mass and moisture fluxes calculated by the model. We have found that in order to simulate precipitation accurately using our new convective parameterization, it is necessary to account for non-buoyantly induced (i. e. stable) precipitation processes. Measurements of precipitation cannot easily distinguish "stable" from "unstable" precipitation. However, models of buoyantly-induced convection cannot properly simulate "stable" precipitation. We have found that during the GATE convective measurements, we see precipitation is excess of what can be accounted for by convective processes, and therefore hypothesize that some of the observed precipitation may result from "stable" processes not directly related with buoyant mechanisms. Therefore, we will develop a "stable" precipitation calculation mechanism, which when used with our convective precipitation parameterization will be capable of forecasting the observed total precipitation rate.

Eventually, we hope to use the improved parameterizations of cloud coverage in a mesoscale meteorology model. Model forecasts which utilize the observed cloud coverage and depth should be improved relative to forecasts which crudely specify cloud properties. During this period, we anticipate running improved versions of the MM4 meteorological model. We plan to continue to expand our database which includes simultaneous observations of cloud cover and other related meteorology. In addition to the springtime observation period already studied, we will be adding

a summer and winter period using the 3DNEPH and RTNEPH clouds, in conjunction with the mesoscale observational assimilation system described above.

4. Journal articles, Presentations & Conference abstracts resulting from this research

(articles attached as an appendix to this report)

Results of this research effort have been presented at a variety of scientific forums. Dr. Walcek met with Air Force Geophysics Lab scientists two times at Hanscom Air Force Base, and additionally at scientific conferences attended jointly by members of both groups. During these meetings, the PI received valuable feedbacks about our research approach, which was ultimately incorporated into the a Peer-reviewed Journal Publication summarizing these results. Additional and more detailed technical insights about specifying cloud coverage are provided in the attached articles describing this research effort. At all meetings and presentations, support from the Air Force Office of Scientific Research was gratefully acknowledged.

The following is a list of the articles and conference presentations resulting from this research effort:

- Walcek, C. J., 1994: Cloud cover and its relationship with meteorological factors during a springtime midlatitude cyclone. *Monthly Weather Review*, **122**, 1021-1035.
- Walcek, C. J., 1995: Cloud Microphysics in GCM cumulus parameterizations: what ensemble averaged quantities really matter? *Conference on Cloud Physics*, Dallas, TX 15-20 January 1995. American Meteorological Society, 45 Beacon St., Boston, MA 02108, 381-382.
- Walcek, C. J., 1994: Cumulus clouds parameterized as detraining plumes. *10th Conference on Numerical Weather Prediction*, Portland, OR 18-22 July 1994. American Meteorological Society, 45 Beacon St., Boston, MA 02108, 77-78.
- Walcek, C. J., 1993: Cloud cover and its relationship with meteorological factors during a springtime midlatitude cyclone. Cloud Impacts on DOD Operations and Systems 1993 Conference (CIDOS-93), Ft. Belvoir, VA, 16-19 November 1993. D. D. Grantham, Editor, Phillips Laboratory, Directorate of Geophysics, Hanscom Air Force Base, MA 01731-3010, 235-240.
- Walcek, C. J., and Q. Hu 1993: A cumulus parameterization scheme of detraining drafts, *20th Conference on Hurricanes and Tropical Meteorology* San Antonio, TX, 10-14 May 1993. American Meteorological Society, Boston, MA. 345-348.
- Walcek, C. J., 1993: Factors influencing regional-scale cloud cover: Investigations using satellite-derived cloud cover and standard meteorological observations. *Fourth Symposium*

on *Global Change Studies*, Anaheim, CA 17-22 January 1993. American Meteorological Society, 45 Beacon St., Boston, MA 02108, 235-236.

Walcek, C. J., 1992: Cloud cover and its relationship with relative humidity during a springtime midlatitude cyclone: some implications for climate models. *Proceedings, 11th International Conference on Clouds and Precipitation*. Montreal, Canada, 17-21 August 1992. Elsevier Publishers, 1128-1131.

Walcek, C. J., 1992: Extrapolating cloud-scale microphysical, dynamic, and radiative processes to global and climatic scales: How accurately do we know the fractional area of cloud coverage?. *Workshop proceedings of the WMO Cloud Microphysics and Applications to Global Climate Change Workshop*. Toronto, Canada, 10-14 August 1992.

Appendix:

Preprints of publications and conference abstracts

Cloud Cover and Its Relationship to Relative Humidity during a Springtime Midlatitude Cyclone

CHRIS J. WALCEK

Atmospheric Sciences Research Center, State University of New York, Albany, New York

(Manuscript received 27 July 1992, in final form 26 October 1993)

ABSTRACT

Vertical distributions of fractional cloud coverage derived from the U.S. Air Force 3DNEPH satellite, aircraft, and surface-based analysis are compared with related standard meteorological observations over the eastern United States. Cloud cover and related observations are interpolated onto the identical three-dimensional grid consisting of 15 tropospheric levels at various horizontal resolutions ranging from $(80 \text{ km})^2$ to $(800 \text{ km})^2$ for five local noon periods during a springtime midlatitude cyclone. During the period analyzed, cloud cover maximizes near 900 mb at 35% cloud cover and decreases to near-zero cover at the surface. Above 900 mb, fractional cloudiness gradually decreases to 10%–20% cover at 200 mb. Cloud cover is positively correlated with relative humidity and large-scale vertical velocity, and negatively correlated with wind shear and temperature lapse rate, except in the lowest 100 mb, where cloud cover is weakly correlated with relative humidity, vertical velocity, wind shear, and temperature lapse rate. Mean fractional cloud coverage observed at various relative humidities and pressures is derived from these observations, and resolution-dependent algorithms for estimating cloud coverage from relative humidity are suggested. This analysis suggests that there is considerable uncertainty in measuring or calculating cloud cover and other meteorological factors averaged over large areas, especially in the upper troposphere. However, cloud cover appears to decrease exponentially as humidity falls below 100%, and relative to other layers in the troposphere, the layers 2.5–5 km above the surface contain the highest cloud amounts at the lowest relative humidities, with mean cloud amounts of 30% near 50% humidity at 650 mb. In the upper troposphere, cloud amounts are greater under convectively unstable conditions relative to stable conditions at high relative humidities. In the lower troposphere, high humidity environments where convection is possible contain lower cloud amounts relative to stable conditions at the same relative humidity, which may result from cumulus-induced subsidence of dry air into the lower troposphere under convectively unstable conditions. Using relative humidity alone as an indicator of cloud coverage, cloud amount can be assessed only to within a root-mean-square difference of 15%–30% from the 3DNEPH cloud cover, depending on the resolution at which calculations are performed. Many meteorological, climate, and chemical models of the atmosphere specify cloud amounts less than reported by these observations when relative humidities are less than 90%–95% during this analysis period. This is especially true in the midtroposphere (850–600 mb), where most algorithms specify zero cloud amounts at relative humidities below 60%–80%, while observed cloud amounts range from 20% to 60% at these height and humidity ranges. At humidities close to saturation, current algorithms probably overestimate cloud coverage.

1. Introduction

Microphysical and dynamical processes occurring within clouds significantly influence numerous larger-scale dynamic, radiative, and chemical processes in the troposphere (e.g., Arakawa and Schubert 1974; Ramanathan et al. 1983; Walcek et al. 1990). At any point in the atmosphere, clouds form when the vapor pressure of water exceeds the vapor pressure that would be saturated with respect to liquid water or ice. However, when averaging over large air masses, it is not unusual to observe cloud formation at humidities well below 100% saturation. Small-scale fluctuations in tempera-

ture and/or water vapor concentration can lead to areas where condensation (clouds) occurs even though the concentration of water averaged over a larger air mass may not be saturated at the mean air mass temperature.

In large-scale numerical models of the atmosphere, chemical or meteorological properties can be explicitly resolved only over relatively large air masses, typically several tens to hundreds of kilometers horizontally and approximately 1000 m vertically. It is not unusual to observe temperature and moisture fluctuations within air volumes of this size because of turbulent or convective motions, surface inhomogeneities, terrain, and other factors. These perturbations induce cloud formation on a scale that cannot be resolved by larger-scale models of the atmosphere, requiring regional or global-scale meteorology models to parameterize the radiative, dynamic, and chemical processes of these subgrid-scale clouds. In most parameterizations of

Corresponding author address: Dr. Chris J. Walcek, Atmospheric Sciences Research Center, State University of New York at Albany, 100 Fuller Road, Albany, NY 12205.

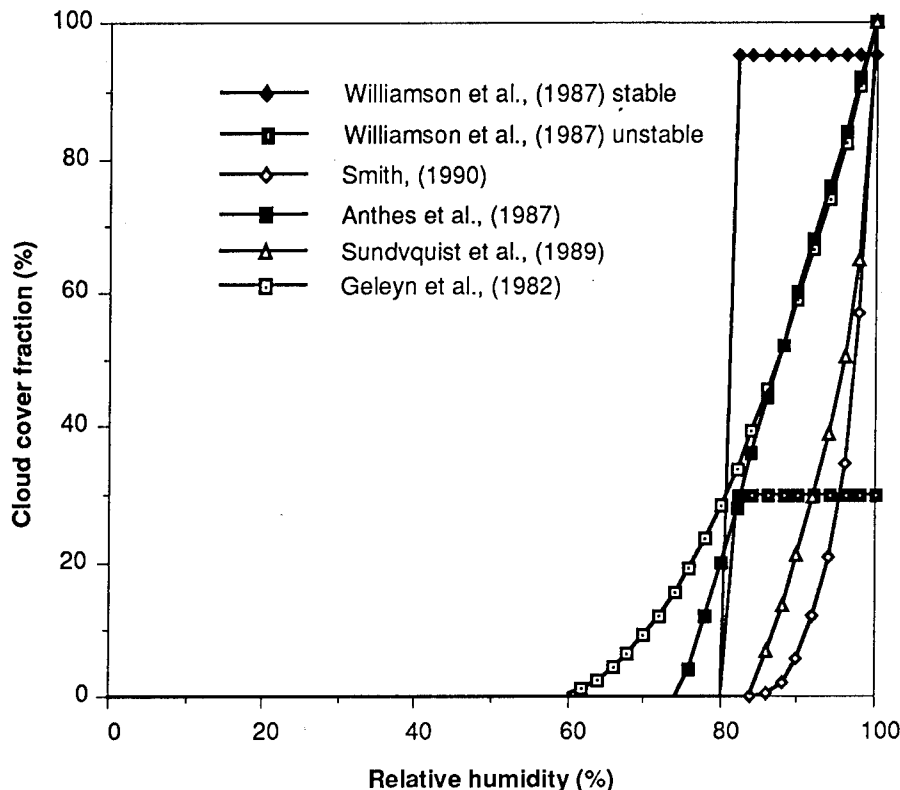


FIG. 1. Fractional cloud coverage as a function of relative humidity at 800 mb according to various formulations used by meso- and global-scale atmospheric models.

cloud-scale processes, the heterogeneous (or subgrid scale) nature of cloudiness is approximated by assuming that a fraction f of each grid area is occupied by clouds. This cloud fraction is used to apportion a significantly different cloud "forcing" into a "grid-averaged" forcing in areas that contain a mixture of clear and cloudy regions.

For this study, cloud cover fraction is defined as the fraction of a given *horizontal* plane in the atmosphere where condensed water is "visibly present" according to standard surface, aircraft, or satellite reports. This definition becomes somewhat vague when "thin" or low condensed water content clouds are present, conditions that commonly occur in the upper troposphere, where it will be difficult to explicitly define or quantify the fractional area of cloud coverage. This definition implies that cloud cover is *vertically varying* and under many conditions may not be directly measurable from either looking up from the surface or down from an aircraft or satellite. The fraction of a downward-looking satellite photograph that is covered with clouds represents a top-down vertical integral of the nonoverlapping fractional area of cloud coverage and essentially ignores lower-level clouds that are covered by higher-level clouds. Similarly, a surface-based observer "sees" a bottom-up integral of the fractional area of

cloud coverage that does not include overlying clouds obscured by lower-level clouds. Deriving a readily observable single cloud cover for one column of the atmosphere would entail knowing information about the overlapping characteristics of f at all levels.

Many studies of clouds and their effects on tropospheric processes have concluded that even small cloud amounts can exert a significant influence on larger-scale processes. Under these conditions, the net impact of clouds on many physical or chemical processes will be proportional to the fractional area of cloud coverage. Most models of tropospheric dynamics assume that the fractional area of cloud coverage is determined by the grid-averaged relative humidity. Figure 1 shows the functional dependence of cloud coverage within a particular atmospheric layer from a survey of formulations currently used by various researchers. All formulations assume a "critical relative humidity" of between 60% and 90%, above which partially cloudy conditions can occur. Below this critical humidity, all algorithms specify totally clear skies. At humidities above the critical humidity, cloud fraction increases by differing functional forms to 100% cloud cover at 100% humidity. Figure 1 shows considerable differences between alternate formulations in assessing cloud coverage within current meteorology and climate models. At 80% hu-

midity, the National Center for Atmospheric Research (NCAR) Community Climate Model (Williamson et al. 1987) specifies 95% cloud cover (under stable conditions), the British Meteorological Office climate model (Smith 1990) uses 0% cloud cover, while other algorithms specify cloud coverage between these extremes.

The uncertainty exhibited in Fig. 1 has motivated researchers to evaluate and improve methods for diagnosing cloud cover. Many researchers have suggested that factors in addition to relative humidity should influence cloud coverage. Using a detailed cumulus ensemble model, Xu and Krueger (1991) find correlations between cloud cover and convective mass flux, convective precipitation rate, and vertical velocity averaged over a large area. To correctly simulate stratiform clouds near large-scale temperature inversions within a global meteorological model, Slingo (1980) hypothesized that cloud cover is influenced by temperature lapse rate. In a study of eastern Pacific marine boundary layer clouds, Betts and Boers (1990) find a correlation between "mixing line stability" and cloud amount. Using a physically intuitive description of cumulus growth and evaporation, Albrecht (1981) finds correlations between trade-cumulus cloud cover and relative humidity and a "virtual saturation ratio," defined approximately as the ratio of the below-cloud water vapor mixing ratio to the saturation mixing ratio within a partially cloudy layer.

In summary, researchers have proposed a wide variety of formulations for estimating cloud cover from related meteorological parameters. Most formulations are derived from a limited set of observations used in conjunction with physically intuitive models of cloud formation. Tunable parameters within cloud cover formulations are empirically adjusted to match a particular (and usually limited) set of observations, or are adjusted within the framework of a larger-scale climatological simulation. For example, Slingo and Slingo (1991) adjust the threshold relative humidities within their cloud cover formulations in order to match climatological estimates of cloud cover and satellite-derived measurements of outgoing longwave radiation.

Relationships between cloud cover and other meteorological factors can be quantified and evaluated using observations of cloud cover and associated meteorology (e.g., Slingo 1980; Sundqvist et al. 1989), or cloud cover can be inferred using fine-resolution dynamic models capable of explicitly resolving cloud-scale dynamics (Xu and Krueger 1991). The primary problem with using observations to infer relationships between cloud cover and other meteorological factors is the difficulty of accurately measuring highly variable and uncertain quantities of interest over relatively large areas. Accurate measurements capable of vertically resolving cloud coverage require high-density vertical soundings, together with satellite and relatively expensive aircraft observations. Due to the expense associated with such

measurement programs, there are only limited observational datasets under a few meteorological environments from which to evaluate and improve cloud cover algorithms.

When models capable of resolving cloud-scale processes are used to ascertain cloud coverage, the accuracy and reliability of the modeling techniques are subject to an independent evaluation, which ultimately relies on observations. Sensitivities of model calculations to the model dimensionality, turbulence and microphysical parameterizations, and other factors must also be evaluated.

As part of an atmospheric chemistry research effort, cloud cover information and related standard meteorological measurements were collected during 20–25 April 1981. This period was chosen since numerous precipitation chemistry and air quality measurements were made during a field experiment over the northeast United States, allowing one to evaluate an atmospheric chemistry model (Middleton et al. 1988). Chemical processes in the troposphere are strongly influenced by clouds, and therefore, it is important to quantify the location, fractional coverage, and vertical distribution of cloud coverage during an atmospheric chemistry simulation. After reviewing several possible mechanisms for specifying cloud coverage within this atmospheric chemical modeling system, it was decided that the cloud observations archived by the U.S. Air Force (3DNEPH) were the best available, and they were already in a format that could be readily used. These cloud cover observations were compiled together with wind, temperatures, and moisture observations into a regularly spaced, simultaneously sampled format during 20–24 April 1981, allowing us to easily compare the cloud cover and related meteorological observations during this period. After reviewing previous studies of clouds and their relationships to other meteorological factors, we concluded that these aggregated observations could possibly contribute to the limited body of simultaneously paired (in time and space) cloud and meteorological observations, and could thus be used to infer relationships between clouds and related meteorological factors.

In this study, we attempt to ascertain the relationships between cloud coverage and other meteorological factors using simultaneous observations of these parameters. Recent attempts to relate *observations* of cloud cover with *observations* of other meteorological factors are limited to a relatively restricted set of meteorological conditions. Much of Slingo's (1980) formulations are inferred from tropical GARP (Global Atmospheric Research Program) Atlantic Tropical Experiment (GATE) observations. Albrecht (1981) considers Atlantic trade-wind cumulus, while Betts and Boers (1990) rely on a single Landsat image of a transitional trade-wind cumulus–stratocumulus area. Sundqvist (1989) qualitatively compares several satellite images with model-calculated cloudiness during

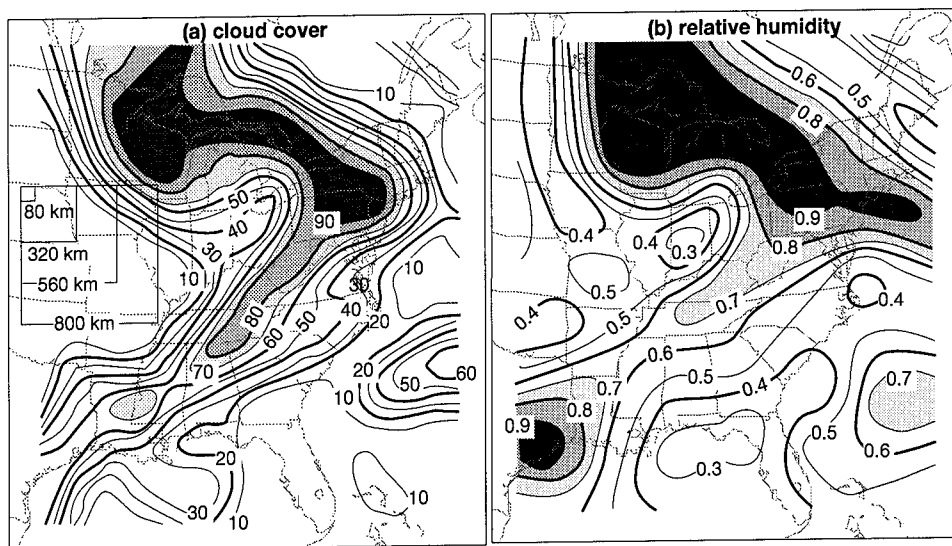


FIG. 2. (a) Cloud cover and (b) relative humidity averaged over $(320 \text{ km})^2$ areas in the layer 800–730 mb at 1800 UTC 23 April 1981. Cloud cover extracted from the U.S. Air Force 3DNEPH compilation of surface reports, aircraft observations, and satellite-derived data. Inset boxes show averaging scales used in this study. Relative humidity interpolated from radiosonde observations in time and space using a hydrostatic mesoscale meteorology model.

a midlatitude cyclone period. We acknowledge beforehand that the standard meteorological parameters and the cloud cover measurements used in this analysis contain a level of uncertainty that is difficult to quantify. However, we feel that the large size of our observational database (relative to previous studies) will allow us to more accurately ascertain the qualitative relationships that may exist between cloud cover and other meteorological factors. By using observations to infer relationships between cloud cover and other meteorological factors, the global-scale influence of cloud microphysical and dynamical processes can be more accurately treated in larger-scale studies of meteorology and atmospheric chemistry.

Meteorological observations used for this analysis are described in section 2. Section 3 provides a summary of the meteorological conditions present during this analysis period, and in section 4, we perform several preliminary statistical surveys of the observations and suggest algorithms for calculating cloud coverage.

2. Description of cloud and meteorology observations

a. Cloud cover

The U.S. Air Force Environmental Technical Applications Center has been receiving and storing Air Force Global Weather Central (AFGWC) cloud data since January 1971. From 1971 to 1983, the AFGWC used an operational real-time three-dimensional analysis of cloud cover referred to as 3DNEPH (Fye 1978). The 3DNEPH is a global analysis of cloud cover that uses surface-based and aircraft reports, together with visual

and infrared satellite imagery, to produce three-dimensional cloud cover information on a routine basis. Cloud fractional coverage is apportioned into 15 different tropospheric levels between the surface and approximately 16 km above the surface based on routine surface reports of the base and top elevation, and cloud cover in the standard low, middle, and high cloud layers. In areas where surface reports are lacking, satellite imagery and aircraft reports are used to estimate cloud coverage and vertical placement. During periods when satellite or surface data are lacking, clouds are inferred from rawinsonde temperatures and dewpoints. The data are mapped onto a polar-stereographic global grid from which we have extracted observations over the northeast United States. Horizontally, the grid size varies from about 25 km near the equator to 60 km at the poles. The 3DNEPH stores cloud cover information every 3 h.

Figure 2a shows an example of the 3DNEPH-analyzed cloud cover averaged over approximately $(320 \text{ km})^2$ areas in the layer 800–730 mb at local noon, 23 April 1981. A broad region of greater cloud coverage corresponding to a warm-frontal region is present over the Great Lakes, and a cold-frontal region extends from Pennsylvania to Texas.

Any cloud cover database will contain a level of uncertainty that is difficult to explicitly evaluate. The 3DNEPH assimilates virtually all routinely available cloud observations, making an independent evaluation impossible. In addition, numerous unevaluated algorithms are used to consolidate surface-based and aircraft observations together with visible and infrared satellite imagery. Hughes and Henderson-Sellers

(1985) performed an analysis of the air force cloud archive for 1979, and although numerous areas of obvious but minor errors were discovered, they found that the cloud observations were generally reliable and in good agreement with known features of tropospheric meteorology. Problems were found when satellite data were gathered over highly variable backgrounds or backgrounds with snow or sea ice. Also, periods of missing data occur, although they are identified. At a minimum, we expect that cloud cover estimates at any given instant in time will contain a level of uncertainty comparable to the uncertainty of surface reports, which report only cloud cover to the nearest octa (12.5%). Chang and Coakley (1993) find that alternate algorithms for extracting cloud cover from infrared satellite imagery over oceanic areas produced mean differences of 18%–25%, depending on the averaging area considered. We expect that this uncertainty is also present in the 3DNEPH algorithms for extracting cloud cover from satellite imagery. Additional errors will be introduced as these cloud amounts are vertically apportioned based on uncertainties in identifying the tops and bases of cloudy layers. Buriez et al. (1988) compared two different methods of analyzing cloud cover from satellite information and found uncertainties ranging from 1.3 to 2.4 octas (16%–30%). When comparing three satellite-derived cloud cover analyses averaged during monthly periods, Mokhov and Schlesenger (1993) find spatial correlation regression coefficients r in cloud cover estimates ranging from 0.52 to 0.85, suggesting a considerable level of uncertainty.

b. Standard meteorology observations

Temperature, moisture, and dynamical data used in this analysis are taken from observations and spatially and temporally interpolated onto an $(80 \text{ km})^2$ Lambert-conformal grid using a hydrostatic mesoscale meteorology model. Observations are derived from the National Meteorological Center global meteorological analysis and further enhanced using 3-h surface observations and 12-h vertical rawinsonde measurements. Vertically, these meteorological data encompass the surface and 100-mb pressure surface ($\sim 16 \text{ km}$), and horizontally, they span the contiguous United States. The vertical grid size of the meteorology data is about 80 m near the surface and on the order of a kilometer or more aloft. These observations are provided as initial and boundary conditions to the NCAR mesoscale meteorological model (MM4, Anthes and Warner 1978). In addition, during model execution, observations are incorporated into the model calculations in regions near observation locations. Differences between observed and calculated temperatures, humidities, and wind speeds are continuously minimized through the use of additional tendency terms in the momentum, moisture, and thermodynamic equations that “nudge” the calculation toward the observations (Stauffer and Seaman

1990). The mesoscale meteorological modeling system is not used to “predict” or “forecast” meteorology. Rather, in a manner suggested by GEWEX (1993), the model interpolates in space and time several meteorological variables of interest in a dynamically and physically reasonable manner. Thus, model calculations agree closely with observations when and where observations are available, and when no observations are available, the meteorological data are dynamically consistent. Under some conditions, meteorology interpolated and analyzed from observations in this manner provides data of superior temporal and spatial resolution relative to “raw,” point observations.

Figure 2b shows the relative humidity in the 800–730-mb layer interpolated from observations using the mesoscale meteorology model described above at the identical time as Fig. 2a. For this figure, temperature and moisture calculations are aggregated into overlapping $(320 \text{ km})^2$ areas, representing a 4×4 average of the 80-km grid used by the MM4. The domain shown in Fig. 2 represents approximately one-half of the domain simulated by the mesoscale meteorological analysis. Comparisons of Figs. 2a,b qualitatively show positive correlations between cloud cover and relative humidity.

Since nearly all routinely available measurements are incorporated into the model calculations, the temperatures, moisture, and dynamic variables resulting from this analysis agree with the measurements to within the instrumental uncertainty. Standard radiosondes are designed to measure temperature within 0.5°C , and relative humidity with an accuracy of 5%–7% (Golden et al. 1986). In addition, radiosonde humidities are known to consistently undermeasure relative humidity under saturated conditions by 2%–4%. Hoehne (1980) found that differences between dewpoint depressions measured by identical radiosondes launched at the same time deviated from one another by $\pm 3.2^\circ$ – 3.7°C . These dewpoint uncertainties alone translate into uncertainties of $\pm 15\%$ – 20% in relative humidity for a typical sounding.

Any method of extrapolating “point” measurements to larger averaging areas will introduce additional uncertainties into the area-averaged “observations.” If a particular radiosonde rises through a cloudy region of a layer of the atmosphere containing a mixture of clear and cloudy areas, it will report approximately 100% humidity for an area where the mean relative humidity would be well below 100%. How often these conditions occur, and just how “noisy” the temperature and water vapor fields are within areas the size of larger-scale model grid areas, is highly variable and (for the period analyzed in this study) uncertain. However, the cloud cover data itself suggests that there is considerable variations from the mean relative humidity within averaging areas larger than $(80 \text{ km})^2$. For example, according to Fig. 2, it is not unusual to see 50% cloud cover at 800 mb when the relative humidity is 60%–

80%. This suggests that within $(320 \text{ km})^2$ averaging areas, when the relative humidity is approximately 70%, fully 50% of the area actually has a relative humidity of 100% (i.e., the cloudy fraction of the grid). Therefore, the likelihood that a radiosonde will rise through an approximately saturated region within this layer is high. At a minimum, the relative humidities used in this analysis contain a level of uncertainty that is probably considerably greater than the raw measurement precision ($\pm 15\%$ – 20%).

3. Description of analysis period

Cloud observations and related meteorology were analyzed over the eastern United States domain during five local noon periods during 20–24 April 1981. At noon, we expect the maximum utilization of aircraft and surface reports together with visual and infrared satellite imagery by the 3DNEPH analysis. Figure 3 shows 700-mb heights and temperatures during the analysis period. On 20–22 April, a ridge of high pressure moved from west to east across the study domain. A trough entered the western portion of the domain on

22 April and rapidly intensified by 23 April. This mid-latitude cyclone continued to intensify and move into the eastern portion of the domain by 25 April. A wide variety of air mass types and temperature regimes were represented during this period. Temperatures at 700 mb ranged from -20° to 15°C , and continental and maritime air with tropical and polar histories were involved in this cyclone.

Figure 4 shows the vertical distribution of relative humidity and cloud cover fraction averaged over the entire domain during the five noon periods shown in Fig. 3. Relative humidities throughout the atmosphere ranged from 20% to 100%, although a majority of the humidities ranged $\pm 30\%$ of the mean humidity. Also shown in Fig. 4a is the global mean relative humidity extracted from an NCAR present-day climate simulation (extracted from a simulation by Wang et al. 1992), showing that the vertical distribution of relative humidity aggregated during this period closely resembles the global mean humidity distribution, suggesting that the meteorological conditions considered in this study do not widely deviate from conditions encountered globally as far as relative humidity is concerned. Figure

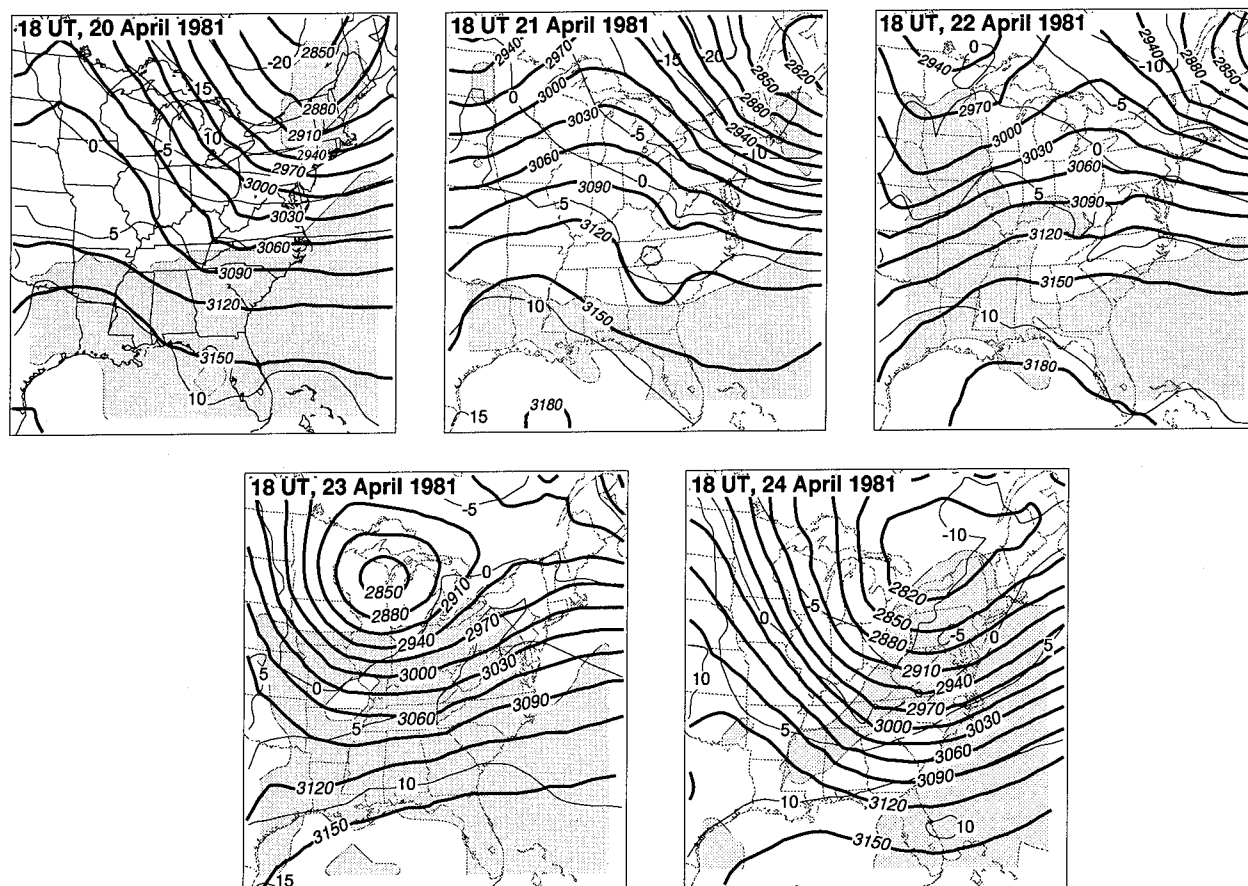


FIG. 3. The 700-mb heights (m, thick solid contours) and temperatures ($^\circ\text{C}$, thin lines) during 20–24 April 1981. Gray areas denote regions where convective motions can potentially occur.

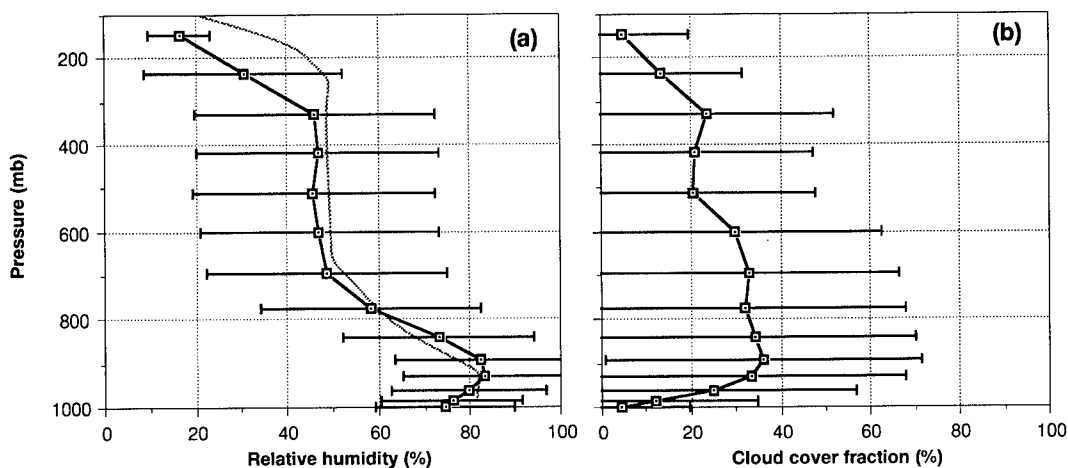


FIG. 4. Vertical distribution of (a) relative humidity and (b) cloud cover fraction averaged over the domain shown in Fig. 3 during 20–24 April 1981. Error bars denote standard deviations about the mean.

5b shows that cloud cover maximizes at about 35% near 900 mb, and gradually decreases to 10%–20% at 200 mb. Cloud amounts ranged from clear to 100%, with a majority of the cloud coverages clustered between 20% and 35% of the mean cloud cover.

Figure 5 shows the temporal deviations from the mean cloud cover and relative humidity averaged over the domain shown in Fig. 3 during 20–24 April 1981.

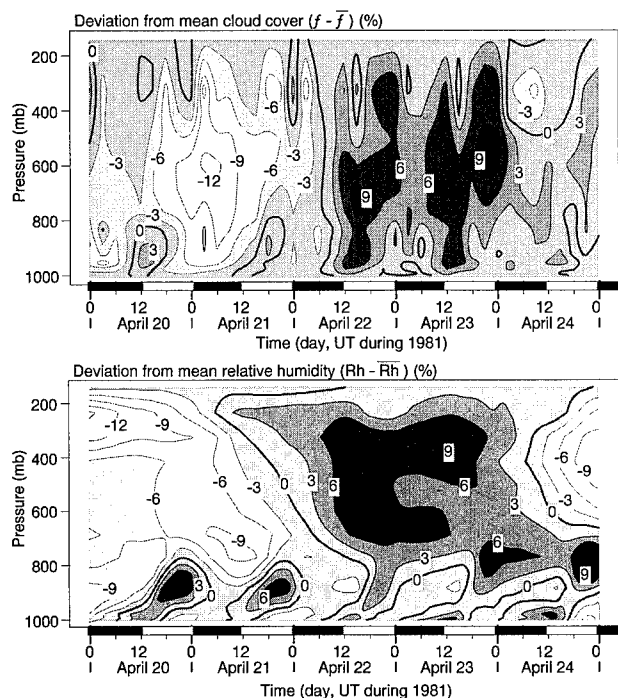


FIG. 5. Temporal variation of (a) cloud cover and (b) relative humidity from the mean values shown in Fig. 4 as a function of height in the troposphere during 20–24 April 1981. Day and night periods are shown as a light or dark strip along time axis.

Dry air is initially present within this domain, and the relative humidity gradually increases downward from upper levels beginning on 21 April. On 24 April, the relative humidity in the upper troposphere rapidly decreases as the cyclone moves out of the domain. The lower atmosphere exhibits a diurnal trend in relative humidity, with peak moistening near the top of the planetary boundary layer during the afternoons. This diurnal pattern is interrupted by the passage of the cyclone through the domain during 22–24 April. Variations in cloud cover correlate approximately with relative humidity variations, with lowest cloud amounts present before the arrival of the midlatitude cyclone, and generally greater cloud fractions during the time when the cyclonic system is centered in the analysis domain.

4. Comparisons between cloud cover and related meteorology

a. General comparisons

Cloud cover and related meteorological observations were mapped onto the identical grid at various horizontal resolutions by area averaging the raw temperature, moisture, or cloud cover data. Horizontal averaging areas were changed from $(80 \text{ km})^2$ to $(800 \text{ km})^2$, corresponding to the approximate range of horizontal resolutions employed by various regional- or global-scale models in use today. Relative humidities are defined relative to the saturation mixing ratio over liquid water, calculated using the mean water vapor mixing ratio and temperature within an averaging area. Saturation with respect to ice could have been defined, but subsequent analysis showed that relative humidity defined with respect to ice did not correlate any better with cloud amounts than relative humidity defined with respect to liquid water. Vertically, the cloud cover and

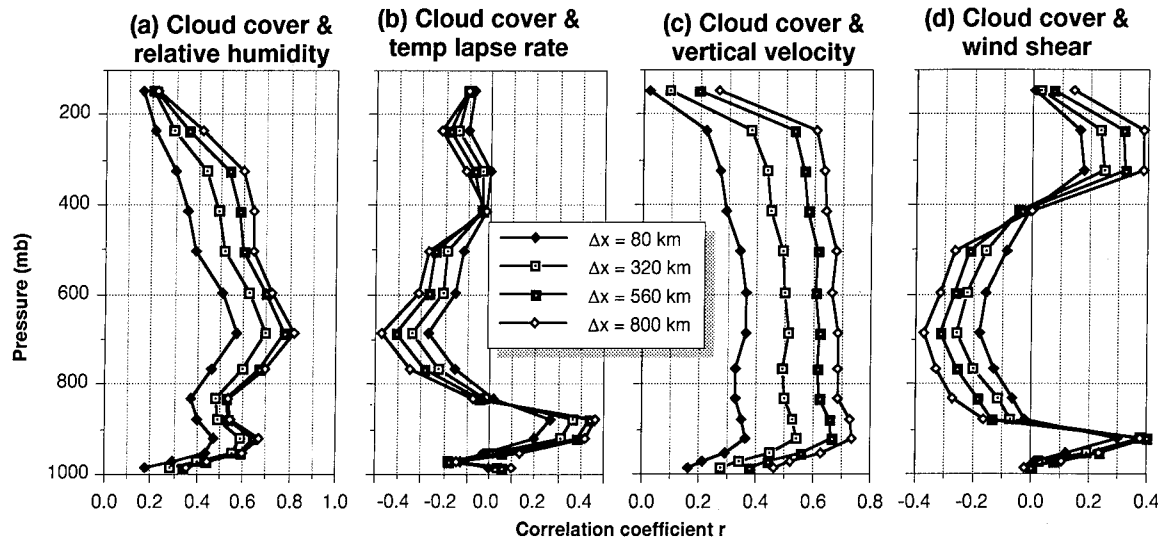


FIG. 6. Correlation coefficient at various atmospheric levels for the best-fit linear relationship between cloud cover and (a) relative humidity, (b) potential temperature lapse rate, (c) vertical velocity, and (d) wind shear. Different curves on each figure denote varying horizontal averaging areas (80–800 km)².

mesoscale interpolation model grids are slightly different, and the cloud cover grid was transposed onto the meteorology model pressure-based coordinate using a cloud-volume-conserving mapping. As a result, a total of 3370–6650 (depending on averaging resolution) data points at 15 tropospheric levels are available for comparison during the five noon periods studied.

The most commonly used indicator of cloud coverage is the mean relative humidity of an air mass. As noted earlier, local potential temperature lapse rate and vertical velocity have also been shown to influence cloudiness. Here we hypothesize that vertical shear of the horizontal wind may also affect cloud cover. Other meteorological factors have been hypothesized to influence cloudiness, although many of these factors are actually model-generated parameters and thus difficult to directly “measure” with routine observations considered in this study. For example, cumulus mass fluxes or “convective” precipitation rates have been used to assess cloud coverage. However, these parameters are difficult to measure directly and will generally have a model-dependent (or resolution dependent) character. In this study, we restrict our comparisons to those parameters that can be readily inferred from routine observations in a straightforward manner.

To evaluate whether any of these parameters are correlated with cloud coverage, we calculate the correlation coefficient for the best-fitting linear regression between cloud cover and each of these meteorological factors for the observations gathered over the domain shown in Fig. 2 for five noon periods during 20–24 April 1981. While we do not expect that any of these parameters will be linearly related to cloud amount, we use this correlation analysis as a means to initially iden-

tify how strongly each of these factors correlates with cloudiness.

Figure 6 shows the vertical distribution of the correlation coefficient for the best-fit linear relationship between cloud cover and humidity, temperature lapse rate, wind shear, and vertical velocity. Correlation coefficients are calculated using all paired observations at each level. Correlation coefficients with magnitudes greater than 0.8 are considered “excellent” according to standard statistical texts, while correlations between 0.6 and 0.8 are considered “good,” and correlations between 0.4 and 0.6 are considered only “moderate.” Correlation coefficients less than 0.4 indicate poor or no relationship between parameters. This figure shows that cloud cover is most strongly correlated (positively) with relative humidity, followed by vertical velocity, which shows moderate to good positive correlations at most tropospheric levels. There is also evidence for a weaker negative correlation between cloud cover and both wind shear and potential temperature lapse rate. Within the planetary boundary layer (lowest 100 mb), cloud cover is weakly positively correlated with nearly all meteorological factors considered here [$0.4 < r < 0.75$ for an averaging area of (800 km)²]. Absolute values of the correlation coefficients increase as the horizontal averaging areas increase, reflecting the decrease in the deviations within the total sample population as larger averaging areas are considered.

Above about 300 mb, we find almost no correlation between cloud cover and other meteorological variables, reflecting the relatively low relative humidity (10%–20%) and cloud cover (0%–20%). At these heights, measurement uncertainty is very large. Routine water vapor measurements are rare above 300 mb, and

therefore, we are relying on purely model-calculated humidities here. In addition, the highest "layers" in this analysis dataset are actually averaged over 3–4-km depths of the atmosphere, and therefore, the "cloud area fraction" defined above actually becomes more like a "cloud volume fraction." Because of this high uncertainty, any trends reported here for the upper troposphere must be interpreted with caution until better measurements are available.

Based on this cursory analysis of factors influencing cloudiness, we conclude that relative humidity and vertical velocity are the best candidates for calculating cloud coverage. However, relative humidity and vertical velocity are themselves strongly correlated, with higher relative humidities usually occurring with upward motions. Even small upward motions will rapidly increase the relative humidity of an atmospheric column since there is such a strong negative gradient of water vapor concentration in the atmosphere. Since relative humidity is a simpler parameter to measure or estimate within larger-scale atmospheric models, we concentrate the following analysis on further studying the relationship between cloud cover and relative humidity.

b. Cloud coverage and relative humidity

The relationship between cloud cover and relative humidity during this analysis period is assessed by aggregating the observations into increments of relative humidity and cloud cover at each level. Figure 7a shows a joint probability distribution (a "smoothed" scatter diagram) of the 3DNEPH cloud cover and interpolated relative humidity observations in the layer between 800 and 730 mb, averaged over $(320 \text{ km})^2$ areas. Contours in this figure show the percent probability of observing relative humidity and cloud cover within a particular 5% increment of either of these parameters.

A high degree of scatter is immediately evident in this comparison between cloud cover and humidity. For example, at 80% relative humidity, Fig. 7a shows a nearly uniform probability of observing any cloud fraction, and the average cloud cover at 80% humidity is about 50%. The correlation coefficient for the best linear relationship between cloud cover and relative humidity at this level is 0.6. When averaging over regions of this size, this scatter is not unexpected and is comparable to deviations found with cloud-resolving models (Xu and Krueger 1991). Similarly, using a statistical approach to modeling subgrid-scale variability, Lewellen and Yoh (1993) find up to 20% deviations in cloud cover at the same relative humidity depending on the skewness of the subgrid distribution of water vapor and temperature within averaging areas. In addition, we fully expect cloud amount to be influenced by factors in addition to relative humidity. Finally, as discussed earlier, the uncertainty in these measured

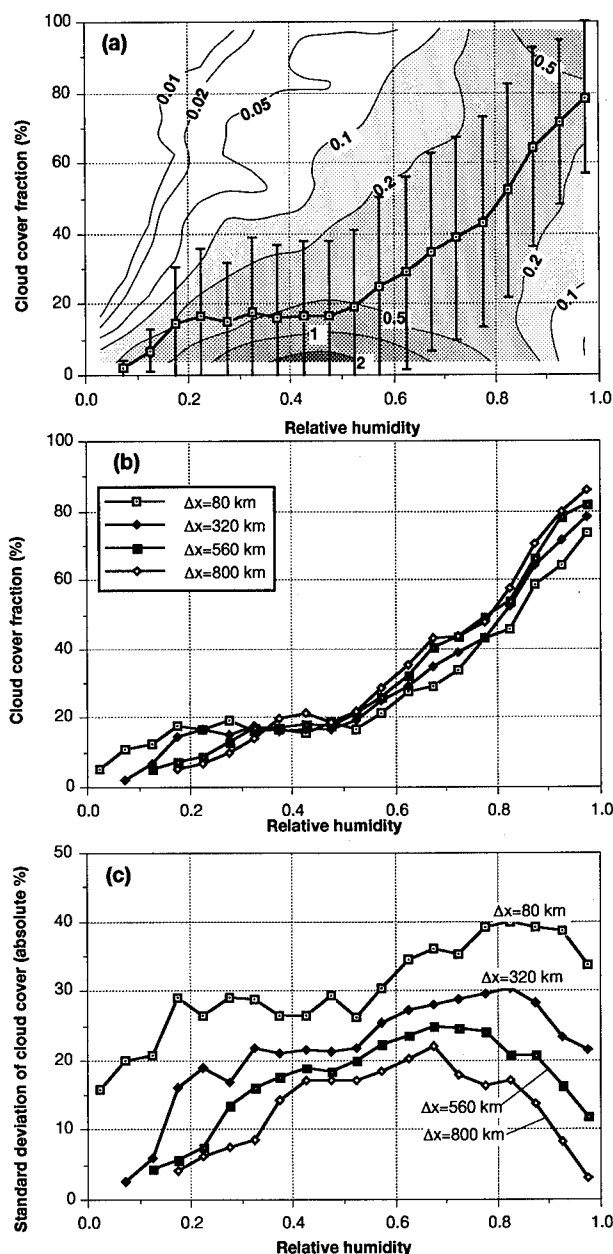


FIG. 7. (a) Joint frequency distribution showing the probability (%) of observing various relative humidity and cloud cover combinations averaged over $(320 \text{ km})^2$ areas in the layer 800–730 mb at five noon periods during 20–24 April 1981. Curve with error bars shows the mean and standard deviation of cloud cover within 5% increments of relative humidity. (b) Mean cloud cover as a function of relative humidity in the 800–730-mb layer for various averaging areas. (c) Standard deviation of the cloud cover within restricted relative humidity ranges at various averaging areas.

cloud amounts and relative humidities is comparable to the range of deviations shown in Fig. 7. However, this high uncertainty does not imply that existing measurements cannot be used to assess relationships between cloud cover and related meteorological factors. If the

sample size for this study is large and covers a wide range of meteorological environments, then trends in cloud cover may be discernible, and the functional relationship between cloud cover and related meteorological parameters may be at least qualitatively revealed.

To assess trends in the measurements shown in Fig. 7a, we aggregate the observations into 5% relative humidity increments at each atmospheric level, then average the cloud coverage within these restricted humidity ranges. Using this averaging technique, trends become apparent in the highly scattered observations. The average and standard deviation of the cloud coverage within 5% relative humidity increments are shown as a curve with error bars in Fig. 7a. As expected, cloud amount increases as humidity increases. At humidities 20%–40%, there is 10%–20% cloud cover on average. We hypothesize that if cloud coverage is related to relative humidity, then that relationship should fall within the range of (and most likely near the middle of) the mean and deviations shown in Fig. 7a.

Figure 7b shows the mean cloud cover within 5% relative humidity increments for horizontal averaging areas ranging from $(80 \text{ km})^2$ to $(800 \text{ km})^2$. All trends show a gradual falloff of cloudiness as relative humidity decreases, and when extrapolated to 100% relative humidity, we see that cloud cover does not necessarily approach 100%. Cloud amounts less than 100% are frequently reported when relative humidities are 100%. At humidities greater than 50%, cloud amount tends to increase as the averaging area increases, since the probability of encountering larger deviations from the mean increases as one averages over a wider area. Figure 7c shows the standard deviations of cloud cover within each increment of relative humidity for the entire population of samples considered in this study. As one averages over larger areas, the ranges of the averaged relative humidities and cloud cover encountered decrease substantially within this fixed domain. Within $(80 \text{ km})^2$ averaging areas at 80% humidity, we see approximately 45% cloud cover, $\pm 40\%$. In contrast, within $(800 \text{ km})^2$ averaging areas at the same relative humidity, we see about 53% cloud cover, $\pm 15\%$.

This process of averaging is repeated at all tropospheric levels to obtain the average cloud cover within each layer at any particular relative humidity, shown in Fig. 8a. At a particular relative humidity, cloud amounts are greatest in the 800–500-mb layer of the troposphere, a trend that is consistent with earlier approximations (Buriez et al. 1988; Geleyn et al. 1982). The highest cloud amounts occur under high humidities at 800–700 mb, but this figure shows that 10%–20% cloud coverage occurs at humidities as low as 20%, in contrast to the formulations shown in Fig. 1, which all specify zero cloud cover at humidities below 60%–80%. Standard deviations of cloud coverage within these 5% humidity increments (Fig. 8b) fall between

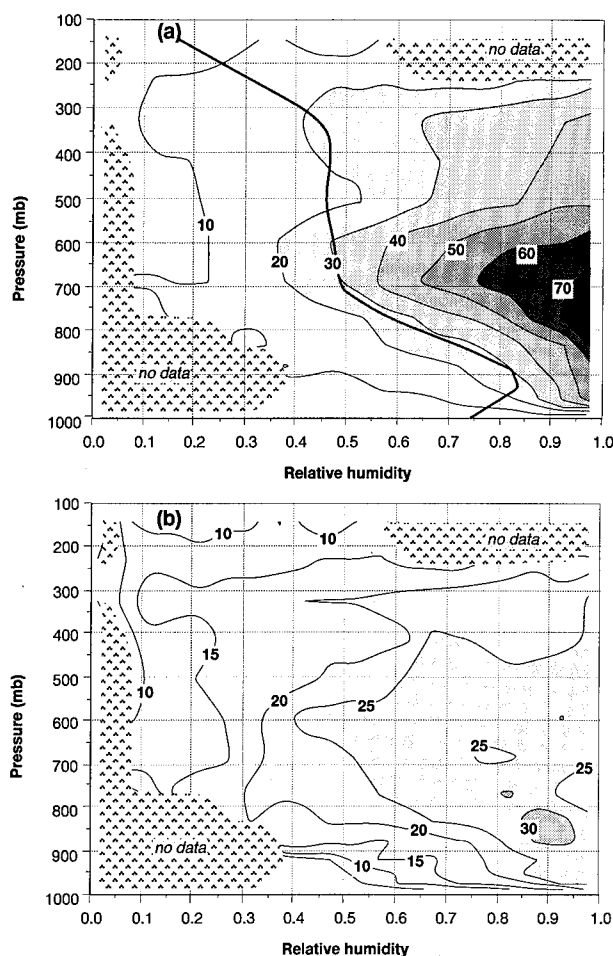


FIG. 8. (a) Mean fractional cloud coverage and (b) standard deviation of fractional cloud coverage observed at various relative humidities and pressures during 20–24 April 1981 over the northeast United States (domain shown in Fig. 2). Curve shown in Fig. 2a shows mean relative humidity during analysis period.

20% and 30% in absolute cloud cover, which in many cases is comparable to the mean cloud cover at this averaging resolution $[(320 \text{ km})^2]$.

The trends in the average cloud amount shown in Figs. 7 and 8 suggest that fractional area of cloud coverage decreases exponentially as the relative humidity falls below 100%, and that there is no clear “critical relative humidity” where cloud coverage is always zero. Also, these trends suggest that at 100% humidity, cloud cover can be significantly lower than 100%. As noted previously, there is a consistent undermeasurement in relative humidity by 2%–4% under saturated conditions, a bias that cannot account for the larger deviations (0%–40%) from 100% cloud cover observed here. Cloud amounts significantly less than 100% at saturation were also noted by Xu and Krueger (1991) within a field of simulated convective clouds. Using a cumulus ensemble model, they found, when averaging over an individual layer of the atmosphere

at resolutions ranging from $(60 \text{ km})^2$ to $(256 \text{ km})^2$, stratiform cloud amounts at 100% humidity well below 100%. The trends in the average cloud amount shown in Figs. 7 and 8 suggest the following approximation for cloud amount f as a function of relative humidity RH ($\text{RH} < 1$):

$$f(\%) = \min \left[f_{100} \exp \left(\frac{\text{RH} - 1}{1 - \text{RH}_e} \right), 100 \right], \quad (1)$$

where f_{100} is the cloud cover extrapolated to or at 100% relative humidity, and RH_e (e -folding relative humidity) is qualitatively similar to the "critical humidity" used in previous cloud cover formulations, although here it represents the relative humidity depression below 100% where cloud amount decreases to 37% (e^{-1}) of its value at 100% humidity.

Using (1) as the functional form that appears to match the qualitative trends noted in Figs. 7 and 8, we calculated the root-mean-square difference between calculated and observed cloud cover for all observations using all combinations of f_{100} and $(1 - \text{RH}_e)$. Figure 9 shows the best values for f_{100} (Fig. 9a) and $(1 - \text{RH}_e)$ (Fig. 9b), along with the corresponding root-mean-square difference $\{[n^{-1} \sum (\text{calculated} - \text{observed})^2]^{1/2}\}$ between the calculated and observed cloudiness. Both of these parameters exhibit a pressure dependence, which we quantify here as the ratio of the pressure P to the surface pressure P_s , and are also slightly influenced by the averaging area $(\Delta x)^2$. The optimum values for f_{100} maximize near about 700 mb and also increase as the averaging dimension increases. The peak value for f_{100} can be approximated by

$$f_{\max}(\%) = 78 + \frac{\Delta x (\text{km})}{15.5},$$

$$80 \text{ km} < \Delta x < 800 \text{ km}. \quad (2)$$

Above about 700 mb, f_{100} falls off from this peak value linearly to zero at $P/P_s = 0.1$:

$$f_{100} = f_{\max} \frac{(P/P_s - 0.1)}{0.6}, \quad 0.7 > \frac{P}{P_s} > 0.1. \quad (3)$$

Below 700 mb, f_{100} decreases to about 30% at the surface:

$$f_{100} = 30 + \frac{(1 - P/P_s)(f_{\max} - 30)}{0.3},$$

$$1 > \frac{P}{P_s} > 0.7. \quad (4)$$

The $(1 - \text{RH}_e)$ term in (1) shown in Fig. 9b linearly increases throughout the depth of the troposphere and is also influenced slightly by the grid resolution. We suggest the following form:

$$(1 - \text{RH}_e) = 0.196$$

$$+ \left[0.76 - \frac{\Delta x (\text{km})}{2834} \right] \left(1 - \frac{P}{P_s} \right). \quad (5)$$

The linear forms for (2)–(5) at a 560-km resolution are shown as lines in Figs. 9a,b. Using (1)–(5) to calculate cloud cover from relative humidity produced cloud cover estimates that on average contained a root-mean-square difference of 20–30 percentage points from the 3DNEPH observations, depending on the tro-

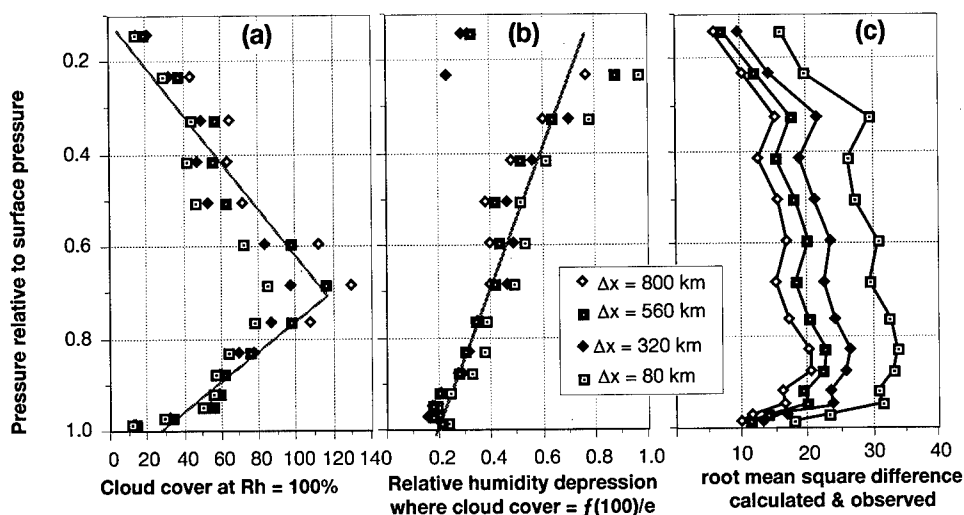


FIG. 9. Optimum values of parameters used to calculate cloud cover from relative humidity. (a) Cloud cover when relative humidity is extrapolated to 100% [Eqs. (3) and (4)]. (b) Relative humidity depression where cloud cover is $1/e$ of cloud cover at 100% humidity [Eq. (5)]. (c) Root-mean-square difference between observed cloud cover and cloud cover calculated using Eqs. (1)–(5). Shaded line in (a) and (b) shows suggested linear fit to optimum values for a horizontal resolution of 560 km.

pospheric level and horizontal averaging area considered. This difference is comparable to previously cited uncertainties in measurements of cloud cover; however, the functional form and sensitivity of cloud cover to changes in relative humidity mimic the observations gathered in this study.

c. Cloud coverage and convective instabilities

We expect cloud coverage to be influenced by the presence of buoyantly induced convection that is not resolved by the coarse resolution of the interpolated observations used in this analysis. Local stability ($\partial T / \partial z$) at any point in a sounding is not a sufficient indicator of the presence of convective activity, since convection can often penetrate into atmospheric layers that are absolutely stable with respect to vertical perturbations (Stull 1991). To define areas and layers where buoyantly induced convection can occur, we provide a 1 m s^{-1} "push" to air with a slightly higher temperature and moisture content from each point on a vertical sounding. In a conditionally unstable environment, the "pushed" parcel will accelerate upward. Ignoring frictional forces and pressure perturbations, the parcel velocity at levels above the layer where it is perturbed can be obtained by integrating the vertical equation of motion for a parcel rising under the influence of buoyant accelerations:

$$\frac{dw}{dz} = \frac{g}{w} \left(\frac{T_{vp} - T_{ve}}{T_{ve}} - q_l \right), \quad (6)$$

where w is the parcel vertical velocity, T_{vp} is the virtual temperature of the rising parcel, T_{ve} is the virtual temperature of the surrounding environment through which the parcel rises, and g is the gravitational acceleration. The condensed water content of the parcel (q_l) is the total water content (assumed to remain constant) of the parcel minus the saturated vapor mixing ratio at any level above the lifting condensation level. For this study, we define a given layer to have a potential for convective clouds if any parcel is capable of rising adiabatically into or through that layer from lower layers under the influence of buoyant forces. These convectively unstable areas at 700 mb are shaded in Fig. 3.

Figure 10 shows the average cloud cover subdivided into $(320 \text{ km})^2$ stable (Fig. 10a) and convectively unstable (Fig. 10b) areas as a function of the layer relative humidity and pressure. Figure 10c shows the difference between the stable and unstable cloud covers ($f_{\text{stable}} - f_{\text{unstable}}$) at the same relative humidity and pressure. Shaded areas in Fig. 10c denote regions where unstable cloud amounts are greater than stable cloud amounts. Since the observations from which these figures are constructed contain a high level of scatter, some of the differences between stable and unstable cloud covers may not be statistically significant. Therefore, we perform a chi-square analysis of these differences. At each

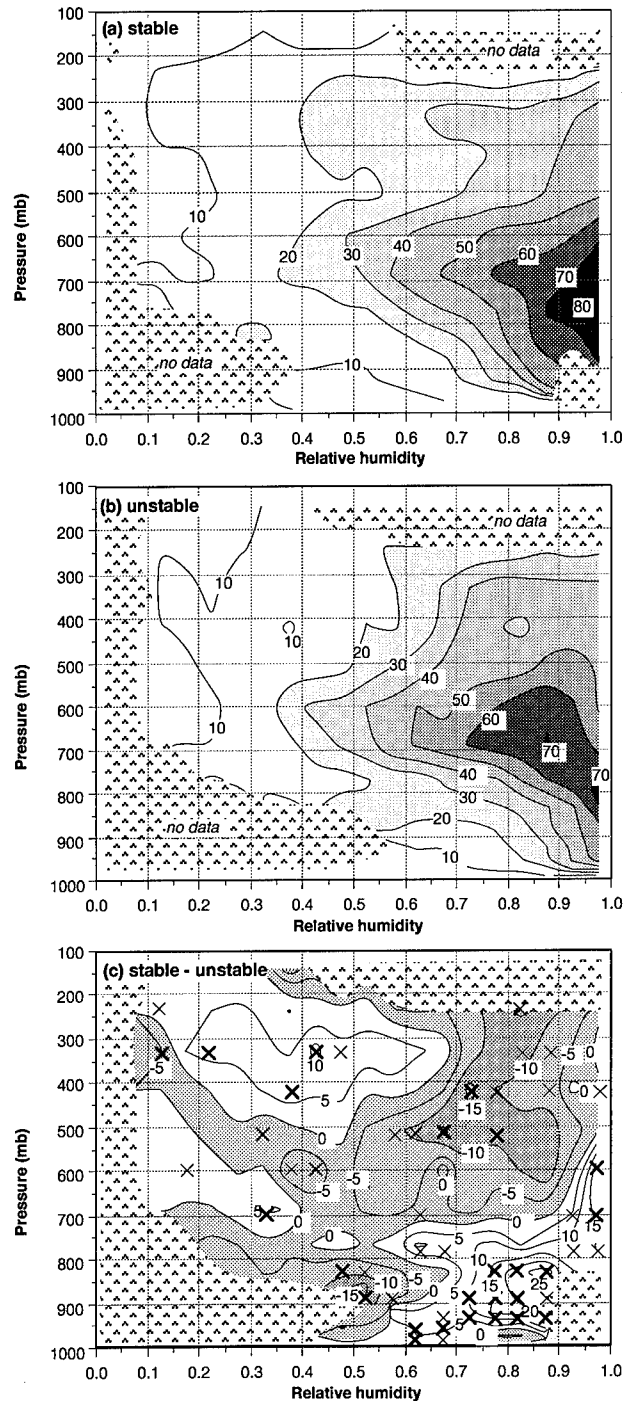


FIG. 10. Comparison of fractional cloud coverage under (a) stable and (b) convectively unstable conditions as a function of relative humidity and pressure during 20–24 April 1981 over the northeast United States (domain shown in Fig. 2). (c) Difference between stable and unstable cloud cover ($f_{\text{stable}} - f_{\text{unstable}}$). Boldface crosses denote differences that are significant with greater than 95% confidence, and lightface crosses denote differences that are significant above only 90% confidence. All other areas contain differences that are significant at less than 90% confidence. Shaded areas in (c) show areas where cloud cover is greater under convectively unstable conditions relative to stable conditions at the same pressure and relative humidity.

atmospheric level, relative humidity and cloud cover data pairs were aggregated into 10% cloud cover increments and 5% humidity increments. The unstable and stable cloud cover frequency distributions were then subjected to a chi-square confidence limits test. Differences between stable and unstable cloud cover that are significant at greater than the 95% confidence limit are denoted by boldface crosses in Fig. 10c, and differences that are significant at greater than the 90% limit are denoted by lightface crosses. Differences that are not close to a cross in Fig. 10c are usually small and may not be statistically significant.

Figure 10c shows that under relatively humid convectively unstable conditions, we see greater cloud amounts relative to stable conditions at the same humidity in the upper troposphere. In the lower troposphere, high humidity environments where convection is possible contain lower cloud amounts relative to stable conditions at the same relative humidity, which may result from cumulus-induced subsidence of dry air into the lower troposphere under convectively unstable conditions. At lower humidities in the lower troposphere, the presence of buoyantly induced convection leads to greater cloud cover. These differences seem physically reasonable. However, under unstable conditions there is a region of significantly lower cloud amounts when humidities are below 65% in the upper troposphere that cannot be easily explained. This anomalous behavior prompted a further investigation of the cloud cover and humidity data. Further analysis of the MM4 interpolation system showed that under unstable conditions, the upper troposphere is calculated to become rapidly saturated when observations are *not* assimilated into the model forecast equations (i.e., the MM4 is run in a "forecast" mode away from the model initial conditions and boundaries). The MM4 calculates humidities approaching 80%–100% in the layer from 500 to 100 mb over regions of mean upward motion and convective activity associated with transient cold and warm fronts. Simultaneous observations show much smaller regions of humidities in excess of 80% between 500 and 300 mb, and there are no measurements above 300 mb, suggesting a bias (overprediction) of relative humidity. Any biases introduced by the model physics into the interpolation of water vapor are partially deleted since water vapor calculations are continuously "nudged" toward the observations for the version of the model used in this analysis. However, above 400–300 mb, there are few humidity observations. Even below 300 mb, despite this "nudging," there may be a residual bias in the MM4 interpolated moisture calculations in these areas. If the "interpolated" relative humidities above 400 mb are higher than were actually present, then this could account for the analyzed reduction in cloud cover under unstable, dry conditions in the upper troposphere. Because of these apparent discrepancies, we feel that the observation–interpolation system described above may introduce a moist bias

in relative humidity in the upper troposphere under unstable conditions. This apparent discrepancy may also influence humidity "measurements" reported here under stable conditions in the upper troposphere, since this is an integrated observation assimilation system, although these errors would be continuously minimized in areas where observations are available. However, as noted earlier, direct measurements of water vapor in the upper troposphere are not available, and we suspect a model-induced bias only because of the apparently lower cloud amounts observed at heights above 400 mb under unstable conditions. Whether this bias is real can be ascertained only with better measurements and evaluations of the MM4 mesoscale meteorology model.

These comparisons of stable and unstable areas at constant heights and relative humidities suggest that convective motions induce large and statistically significant changes in cloud cover. In the lower troposphere, convection increases cloud cover under dry conditions ($RH < 60\%$ – 70%) and decreases cloud cover under moist conditions ($RH > 60\%$ – 70%). In the moist upper troposphere ($RH > 60\%$), cloud cover is greater when convection is occurring, although these trends may be biased due to an apparent bias in our ability to infer relative humidities in the upper troposphere. As noted by previous researchers, there is most likely a relationship between convective mass fluxes or convective precipitation rate and cloud cover under unstable conditions. However, using routinely available meteorological measurements, it is difficult to quantify either of these measures of convective intensity. When we analyze cloud cover within a relatively constant and narrow relative humidity range, we find no correlations between cloud cover and convective available potential energy (CAPE), a standard measure of convective instability. These initial comparisons suggest that diagnosing the effects of convection on cloud cover is very complicated, requiring further study using more accurate measurements of cloud cover and relative humidity.

5. Discussion and conclusions

In this study, we have compared satellite observations of fractional cloud coverage with related meteorological observations over the northeast United States during a springtime midlatitude cyclone. Cloud cover observations were derived from the U.S. Air Force 3DNEPH analysis of satellite imagery, aircraft reports, and surface-based observations. Other meteorological measurements were interpolated from radiosonde observations using a hydrostatic mesoscale meteorology model. Collocated comparisons of the cloud cover with other meteorological measurements show considerable uncertainty, although we find moderate to good correlations between cloud cover and relative humidity and vertical velocity. An analysis of the relationship between observed cloud cover and humidity

suggests that cloud cover decreases exponentially as humidity falls below 100%. Relative to other layers in the troposphere, the midtroposphere (700–500 mb) contains higher cloud amounts at the lowest humidities, with mean cloud amounts of approximately 30% near 50% humidity. Cloud cover also exhibits weak negative correlations with potential temperature lapse rate and vertical shear of the horizontal wind in the middle atmosphere. Throughout most of the troposphere, relative humidity is the best *single* indicator of cloud coverage, and resolution-dependent formulations that calculate the cloud cover from relative humidity are presented.

Under conditions when buoyantly forced vertical motions are possible, cloud cover is greater in the upper troposphere and smaller in the lower troposphere when relative humidity is greater than about 60%. However, anomalous low cloud amounts under unstable conditions are recorded at low humidities above about 400 mb, suggesting that model-interpolated relative humidity may be biased there. Thus, the 3DNEPH cloud observations are being used as an evaluation tool. In a manner similar to Nehr Korn and Hoffman (1990), this analysis suggests that cloud coverage may be a useful tool for inferring relative humidity, contrary to the underlying purpose of most cloud cover algorithms: to infer cloud coverage from other “easy to estimate” meteorological factors. For inferring upper-tropospheric water vapor concentrations, perhaps cloud observations are easier to estimate with greater accuracy than relative humidity.

Despite the high level of uncertainty present in this analysis of cloud cover, most parameterizations of cloud coverage used by current meteorology and climate models yield smaller cloud amounts than reported by the 3DNEPH at particular relative humidities, especially in the midtroposphere. Near 800 mb when the relative humidity is near 70%–90%, many cloud cover formulations (shown in Fig. 1) specify cloud cover fractions considerably lower than the mean minus one standard deviation from the measurements presented in Fig. 7. At humidities below 60%–80%, nearly all algorithms specify zero cloud coverage, while the 3DNEPH reports 10%–20% cloud cover at humidities as low as 20%, although the zero cloud amount used by most algorithms falls within the standard deviations (and uncertainties) of the observations.

We find no evidence for “threshold” relative humidities below which cloud cover is always zero. Previous observational analyses and modeling studies have actually extrapolated the trends measured within relatively narrow (and moist) humidity ranges outside the ranges where measurements were available, thus generating a need for a “threshold humidity.” For example, Slingo (1980) noted a trend in low cloud cover when the relative humidity was 65%–90%. However, Slingo’s cloud observations were confined to periods when relative humidities were confined to the 65%–

90% range, making it impossible to infer cloud cover under drier conditions. In this study, the relative humidity at any atmospheric level showed considerably greater range than reported in previous studies, and in particular we have sampled periods and areas when relative humidities are considerably lower than 70%. Thus, the observations presented here do not necessarily disagree with previous observational studies, but these observations are gathered over a wider range of environmental conditions.

Many of the formulations for cloud cover used by climate models are not actually based on short-term observations of cloud cover and relative humidity. Rather, these formulations along with their “critical humidities” are “tuned” within the context of their host model physics and dynamics to yield reasonable estimates of the global, long-term planetary outgoing longwave radiation or albedo. Thus, cloud cover formulations are “backed out” of their host model, and represent a functional form that when used in the particular climate model for which they were tuned, yield a reasonable planetary albedo and/or outgoing longwave radiation. The danger of this method of assessing cloud cover is that other model uncertainties or errors may be concealed by an incorrect cloud cover formulation. For example, forcing model clouds to be smaller can conceal excessively large optical depths. Slingo and Slingo (1991) find that when increasing the resolution of a climate model, it was necessary to reduce the “critical relative humidities,” thus increasing cloud amounts at humidities above 70%–90% and allowing clouds to form at lower humidities. This behavior is the opposite of the results presented in this study. Figure 7 shows that at a fixed relative humidity, as the averaging resolution increases (Δx smaller), cloud amounts decrease since the dispersion about the mean relative humidity decreases as one reduces the averaging area, decreasing the likelihood that saturated conditions exist within the averaging area.

These results suggest that current methods of calculating cloud coverage within large-scale climate simulations or atmospheric chemical modeling studies are probably underestimating cloud amount at most relative humidities. More importantly, current climate models probably cannot adequately estimate the potentially significant *changes* in cloud cover that can result from small changes in relative humidity. As clearly shown in Fig. 1, a small change in relative humidity can result in large or small changes in cloud coverage, depending on which cloud cover algorithms are used. This analysis of the 3DNEPH cloud archive shows an exponentially decreasing cloud cover as relative humidity decreases, and no clear “critical relative humidity” below which there are no clouds. According to the trends revealed by this analysis, cloud amount probably changes as relative humidity changes at *any* relative humidity, unlike current formulations, where cloud cover changes when relative humidity is greater than

the 60%–90% “critical” humidities used by current cloud cover formulations.

Acknowledgments. The author is grateful to the organizations that are supporting portions of the research presented here: the U.S. National Science Foundation under Grant ATM-9014933; the U.S. Department of Energy under Grant DE-FG02-92ER61364; and the U.S. Air Force Office of Scientific Research under Grant F49620-92-J-0018.

REFERENCES

- Albrecht, B. A., 1981: Parameterization of trade-cumulus cloud amounts. *J. Atmos. Sci.*, **38**, 97–105.
- Anthes, R. A., and T. T. Warner, 1978: Development of hydrodynamic models suitable for air pollution and other mesometeorological studies. *Mon. Wea. Rev.*, **106**, 1045–1078.
- Arakawa, A., and W. H. Schubert, 1974: Interaction of a cumulus ensemble with the large-scale environment, Part 1. *J. Atmos. Sci.*, **31**, 674–701.
- Betts, A. K., and R. Boers, 1990: A cloudiness transition in a marine boundary layer. *J. Atmos. Sci.*, **47**, 1480–1497.
- Buriez, J.-C., B. Bonnel, Y. Fouquart, J.-F. Geleyn, and J.-J. Morcrette, 1988: Comparison of model-generated and satellite-derived cloud cover and radiation budget. *J. Geophys. Res.*, **93**, 3705–3719.
- Chang, F.-L., and J. A. Coakley, 1993: Estimating errors in fractional cloud cover obtained with infrared threshold methods. *J. Geophys. Res.*, **98**, 8825–8839.
- Fye, F. K., 1978: The AFGWC automated cloud atlas model. AFGWC Tech. Memo. 78-002. HQ Air Force Global Weather Central, Offutt AFB, NE, 58 pp.
- Geleyn, J.-F., A. Hense, and H.-J. Preuss, 1982: A comparison of model-generated radiation fields with satellite measurements. *Beitr. Phys. Atmos.*, **55**, 253–286.
- GEWEX Science Team, 1993: The GEWEX cloud system study (GCSS) 1993. *Bull. Amer. Meteor. Soc.*, **74**, 387–399.
- Golden, J. H., R. Serafin, V. Lally, and J. Facundo, 1986: Atmospheric sounding systems. *Mesoscale Meteorology and Forecasting*, P. S. Ray, Ed., Amer. Meteor. Soc., 50–70.
- Hoehne, W. E., 1980: Precision of National Weather Service upper air measurements. NOAA Tech. Memo. NWS T&ED-16, National Weather Service, 23 pp. [NTIS PB81-108136.]
- Hughes, N. A., and A. Henderson-Sellers, 1985: Global 3D-nephanalysis of total cloud amount: Climatology for 1979. *J. Appl. Climate Meteor.*, **24**, 669–686.
- Lewellen, W. S., and S. Yoh, 1993: Binormal model of ensemble partial cloudiness. *J. Atmos. Sci.*, **50**, 1228–1237.
- Middleton, P., J. S. Chang, J. C. delCorral, H. Geiss, and J. M. Ronsinski, 1988: Comparison of RADM and OSCAR precipitation chemistry data. *Atmos. Environ.*, **22**, 1195–1208.
- Mokhov, I. I., and M. E. Schlesinger, 1993: Analysis of global cloudiness 1. Comparison of Meteor, Nimbus 7, and International Satellite Cloud Climatology Project (ISCCP) satellite data. *J. Geophys. Res.*, **98**, 12 849–12 868.
- Nehrkorn, T., and R. N. Hoffman, 1990: Inferring relative humidity profiles from 3DNEPH cloud data. *J. Appl. Meteor.*, **29**, 1330–1343.
- Ramanathan, V., E. J. Pitcher, R. C. Malone, and M. L. Blackmon, 1983: The response of a spectral general circulation model to refinements in radiative processes. *J. Atmos. Sci.*, **40**, 605–630.
- Slingo, A., and J. M. Slingo, 1991: Response of the National Center for Atmospheric Research Community Climate Model to improvements in the representation of clouds. *J. Geophys. Res.*, **96**, 15 341–15 357.
- Slingo, J. M., 1980: A cloud parameterization scheme derived from GATE data for use with a numerical model. *Quart. J. Roy. Meteor. Soc.*, **106**, 747–770.
- , 1987: The development and verification of a cloud prediction scheme for the ECMWF model. *Quart. J. Roy. Meteor. Soc.*, **113**, 899–927.
- Smith, R. B. N., 1990: A scheme for predicting layer clouds and their water content in a general circulation model. *Quart. J. Roy. Meteor. Soc.*, **116**, 435–460.
- Stauffer, D. R., and N. L. Seaman, 1990: Use of four-dimensional data assimilation in a limited-area mesoscale model. Part 1: Experiments with synoptic-scale data. *Mon. Wea. Rev.*, **118**, 1250–1277.
- Stull, R. B., 1991: Static stability—An update. *Bull. Amer. Meteor. Soc.*, **72**, 1521–1529.
- Sundqvist, H., E. Berge, and J. E. Kristjánsson, 1989: Condensation and cloud parameterizations studies with a mesoscale numerical weather prediction model. *Mon. Wea. Rev.*, **117**, 1641–1657.
- Walcek, C. J., W. R. Stockwell, and J. S. Chang, 1990: Theoretical estimates of the dynamic, radiative and chemical effects of clouds on tropospheric trace gases. *Atmos. Res.*, **25**, 53–69.
- Wang, W.-C., M. P. Dudek, and X.-Z. Liang, 1992: Inadequacy of effective CO₂ as a proxy in assessing the regional climate change due to other radiatively active gases. *Geophys. Res. Lett.*, **19**, 1375–1378.
- Williamson, D. L., J. T. Kiehl, V. Ramanathan, R. E. Dickinson, and J. J. Hack, 1987: Description of the NCAR Community Climate Model (CCM1). NCAR Tech. Note NCAR/TN-285+STR, National Center for Atmospheric Research, Boulder, CO, 112 pp.
- Xu, K.-M., and S. K. Krueger, 1991: Evaluation of cloudiness parameterizations using a cumulus ensemble model. *Mon. Wea. Rev.*, **119**, 342–367.

9A.3 CLOUD MICROPHYSICS IN GCM CUMULUS PARAMETERIZATIONS: WHAT ENSEMBLE-AVERAGED QUANTITIES REALLY MATTER?

Chris J. Walcek

State University of New York, Albany, New York

1. INTRODUCTION

Large-scale meteorology models use relatively crude methods for calculating the effects of cloud microphysics and dynamics on larger-scale atmospheric processes. While current-generation microphysical formulations are capable of explicitly specifying numerous phase transitions among several water categories in cloud updrafts and downdrafts, most larger-scale atmospheric models only need to know heating and total moisture tendencies ($\partial T/\partial t$; $\partial q_v/\partial t$) averaged over an ensemble of clouds within each numerical grid. In this study, we describe a new parameterization of buoyant convection that includes a relatively sophisticated description of cloud microphysics (compared with current cumulus parameterizations). The contributions of various microphysical phase transition processes to larger-scale heat tendencies are presented in the context of some observations of convective tendencies.

2. CONVECTIVE PARAMETERIZATION

Dynamics In this model, buoyantly-accelerated motions are initiated by turbulent impulses of heat, moisture and vertical velocity. In unstable layers, turbulently-"kicked" parcels accelerate up according to:

$$\frac{dw}{dz} = \frac{g}{w} \left[\frac{T_{vp} - T_{ve}}{T_{ve}} - q_l \right] \quad (1)$$

where w is the parcel vertical velocity, T_{vp} and T_{ve} are the virtual temperature of the rising parcel and the surrounding environment, and g is the gravitational acceleration. Adiabatic properties are used for calculating the initial acceleration as well as the height to which buoyantly-dislodged parcels can rise in an unstable column. As buoyantly-accelerated parcels rise, they mix with their surrounding environment. Previous mass-flux models of convection (e. g., Arakawa and Schubert, 1974) assume that cloud-free air is "entrained" into a cumulus updraft and carried upward. However, in moist plumes where condensation and evaporation are occurring, Warner (1970) showed that entraining models of convective clouds are inconsistent with observations.

Due to evaporation of cloudwater, many mixtures of cloud and environmental air become negatively buoyant, and quickly separate from an upward-moving plume. Thus we propose that moist plumes detrain mass as they rise through and mix with a drier environment. This detrainment can be expressed as the following equation describing the mass flux (M_c , $\text{kg m}^{-2} \text{h}^{-1}$) originating from a particular unstable layer:

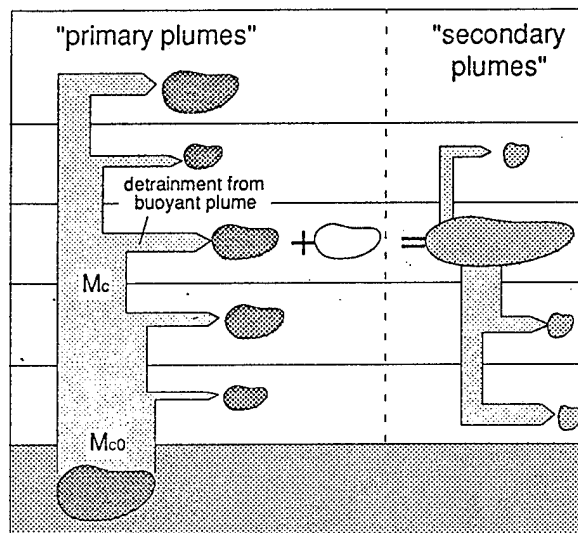


Figure 1. Schematic of convection model.

$$\frac{dM_c}{dz} = -\frac{M_c}{l_d} \quad (2)$$

where l_d is a characteristic "detrainment length" that determines the rate of "shedding" of mass from an upward-moving plume. Observations of convection show that environmental relative humidity and vertical shear of horizontal winds influence l_d . In dry, high-shear environments, greater mixing and evaporation of cloudwater produces more negatively buoyant mixtures, leading to shorter detrainment lengths. Basically, cumulus clouds have trouble penetrating through dry, high-shear layers of the atmosphere.

Fig. 1 shows schematically the motions considered within unstable environments according to this convection model. Air that can accelerate upward from any layer of the atmosphere under the influence of buoyant forces constitutes the "primary", unmixed convective plumes. Air within the primary plumes rises and "sheds" mass according to Eq. (2). Detrained air at each atmospheric level mixes with its environment, producing mixtures that accelerate upward or downward, depending on their buoyancy. Following Raymond and Blyth (1992) we assume that a distribution of mixtures is formed as air is shed from the "primary" updrafts. These mixtures constitute the "secondary plumes" which rise or sink to their level of neutral buoyancy, again shedding mass along the way.

Microphysics Cloudwater or ice will condense as parcels rise under the influence of buoyant forces. Cloudwater either evaporates or coalesces to form

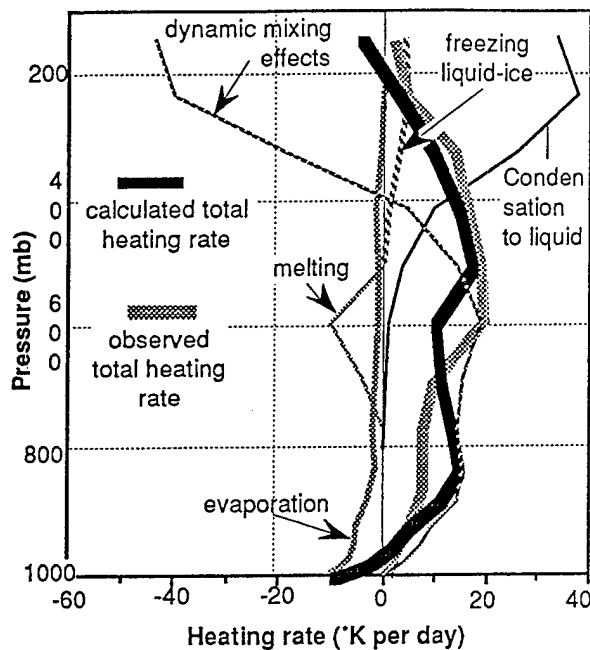


Figure 2. Calculated and observed heating rate ($\partial T/\partial t$ $^{\circ}\text{K day}^{-1}$) due to convection and various microphysical processes in the GATE measurement area at 15 UTC, 2 Sept. 1974.

precipitation. Evaporation is assumed to occur within a time scale that depends on the average relative humidity of the layer where the evaporation is occurring. Following Kessler (1969), precipitation formation also occurs within a characteristic time, and this time scale is reduced above the 0°C level to account for Bergeron growth environments. Melting and evaporation of precipitation are also considered by allowing precipitation to fall out of the saturated updrafts according to the local shear of the horizontal winds.

Using this model one can calculate the precipitation produced for each kilogram of mass moved out of unstable atmospheric layers [$\equiv P_m$ - mm per (kg m^{-2})]. If observations of precipitation rate (Pr - mm h^{-1}) are available within a sufficiently large convectively active area, one can then diagnostically specify the convective mass flux (Mc_0) out of each layer so that the observed precipitation is matched. $Mc_0 = Pr \div P_m$.

The net effect of buoyantly-initiated motions and microphysical processes is to redistribute air within an atmospheric column, and transport or exchange heat, moisture, and momentum among various atmospheric layers, thus changing the temperature, moisture (and wind speed) of all layers affected by convection.

3. MICROPHYSICAL CONTRIBUTIONS

During GATE, the net heating tendencies due to convective processes were indirectly measured within a large area of the tropical Atlantic during Sept. 1974. The bold curves shown on Fig. 2 show the measured and calculated convective heating tendencies during one

convectively active period of GATE. Both the placement and magnitude of the convective-scale heating and moistening tendencies are reasonably simulated by the model described above throughout the GATE measurement period. This heating tendency represents an agglomeration of dynamic and microphysical processes. The numerous smaller curves shown on Fig. 2 show the contributions of these effects to the total tendency.

In the upper atmosphere, upward displacement of lower tropospheric air with lower potential temperature is largely balanced by latent heat release as water condenses and precipitates. Melting of frozen precipitation cools a narrow layer near the 0°C level, while evaporation of precipitation significantly cools the lower atmosphere, nearly compensating for the subsidence heating there.

4. DISCUSSION AND CONCLUSIONS

We have developed a multi-stream model of convection for diagnosing vertical profiles of larger-scale heat ($\partial T/\partial t$) and moisture ($\partial q_v/\partial t$) tendencies attributable to buoyantly-forced motions within an ensemble of convective clouds for use in hydrostatic meteorology and climate models. This parameterization includes effects associated with updrafts and downdrafts, larger-scale subsidence, and generation and evaporation of precipitation using relatively sophisticated treatment of microphysics. The competition between evaporation of cloud water and coagulation to form precipitation plays a key role in determining whether convective clouds heat (& dry) or cool (& moisten) cloudy layers of the atmosphere. This study suggests that larger-scale measurements (such as GATE) can be used to crudely estimate gross features about convective precipitation efficiencies and mass fluxes between atmospheric layers.

Acknowledgments. The authors are grateful to the NSF, AFOSR, and the DOE for supporting this research. Grateful acknowledgments to J. Wang and D. Randall of CSU for providing processed GATE measurements.

REFERENCES

- Arakawa, A. and Schubert W. 1974. Interaction of cumulus cloud ensembles with the large-scale environment part 1. *J. Atmos. Sci.*, 31, 674-701.
- Kessler, E. 1969. On the distribution and continuity of water substance in atmospheric calculations. *Meteorological Monographs*, vol 10, #32. American Meteorological Society, Boston, Mass.
- Raymond, D. and A. Blyth 1992. Extension of the stochastic mixing model to cumulonimbus clouds. *J. Atmos. Sci.*, 49, 1968-1983.
- Warner, J., 1970: On steady-state one-dimensional models of cumulus convection. *J. Atmos. Sci.*, 27, 1035-1040.

FA 3B.5 CUMULUS CLOUDS PARAMETERIZED AS DETRAINING PLUMES

Chris J. Walcek, Qi Hu and Bob Iacovazzi

State University of New York, Albany, New York

1. INTRODUCTION

Most synoptic-scale weather forecast models implicitly ignore cloud-scale vertical motions by using the hydrostatic approximation. However, under many conditions, nonhydrostatic motions can influence larger-scale tropospheric processes, and therefore these "neglected" motions must be accounted for, usually in a simplified or parameterized fashion. In this study, a new physically-based model of buoyant convection is presented to describe the effects of clouds on moisture and heat distributions in the atmosphere. Following a description of the model, the model is evaluated using measurements of convection over the tropical Atlantic.

2. CONCEPTUAL MODEL OF CONVECTION

Dynamics In our model, buoyantly-accelerated motions are initiated by turbulent impulses of heat, moisture and vertical velocity. In unstable layers, turbulently-"kicked" parcels accelerate up according to:

$$\frac{dw}{dz} = \frac{g}{w} \left[\frac{T_{vp} - T_{ve}}{T_{ve}} - q_l \right] \quad (1)$$

where w is the parcel vertical velocity, T_{vp} and T_{ve} are the virtual temperature of the rising parcel and the surrounding environment, and g is the gravitational acceleration. Adiabatic properties are assumed for the calculation of the initial acceleration as well as the height to which buoyantly-dislodged parcels can potentially rise in an unstable column. As buoyantly-accelerated parcels rise, they mix with their surrounding environment. Previous mass-flux models of convection (e. g., Arakawa and Schubert, 1974) assume that air from outside the cloud is "entrained" into the cumulus updraft and carried upward. However, in moist plumes where condensation and evaporation are occurring, Warner (1970) demonstrated that entraining models of convective clouds are inconsistent with observations.

Due to evaporation of cloudwater, many mixtures of cloud and environmental air will be negatively buoyant, and will quickly separate from an upward-moving plume. This explains the typical cumulus cloud shape where the width of the cloud decreases with height. Thus we propose that moist plumes detrain mass as they rise through and mix with a drier environment. Mathematically, this can be expressed as the following equation describing the mass flux (M_c , kg m⁻² h⁻¹) of an ensemble of convective updrafts:

$$\frac{dM_c}{dz} = -\frac{M_c}{l_d} \quad (2)$$

where l_d is a characteristic "detrainment length" that determines the rate of "shedding" of mass from an

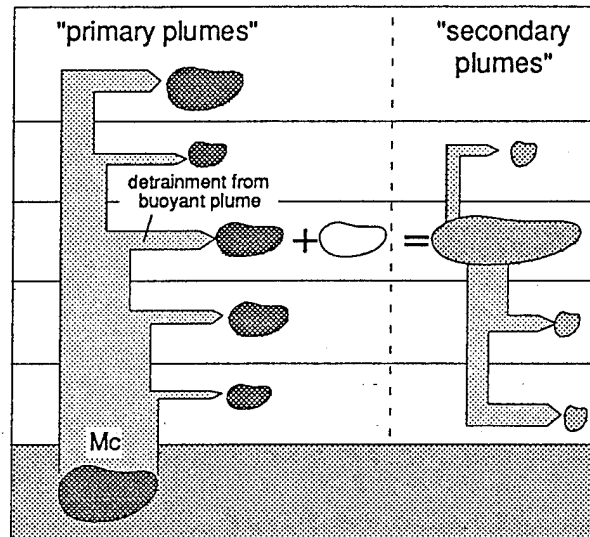


Figure 1. Schematic of convection model.

upward-moving plume. Many factors should influence l_d , but probably the most important is the relative humidity of the environment into which a convective ensemble grows. In a drier environment, greater evaporation of cloudwater will produce more negatively buoyant mixtures, leading to more "detrainment".

Fig. 1 shows schematically the motions considered within unstable environments by our model of convection. Unmixed air that can accelerate upward from any layer of the atmosphere under the influence of buoyant forces (as defined using Eq. 1) constitutes the "primary" convective plumes. Air within the primary plumes rises and "sheds" mass according to Eq. (2). Detrained air at each atmospheric level mixes with its environment, producing mixtures that accelerate upward or downward, depending on their buoyancy. Following Raymond and Blyth (1992) we assume that a uniform distribution of mixtures is formed as air is shed from the "primary" updrafts. These mixtures constitute the "secondary plumes" which rise or sink to their level of neutral buoyancy, again shedding mass along the way. All motions cease as these secondary plumes reach their levels of neutral buoyancy.

Microphysics As updraft air rises and mixes, cloudwater either evaporates or coalesces to form precipitation. Evaporation occurs within a time scale that depends on the relative humidity of the layer where buoyantly-displaced parcels rise. Precipitation formation also occurs within a characteristic time, and is enhanced above the 0°C level. Melting and evaporation of precipitation are also considered.

The net effect of buoyantly-initiated motions is to redistribute air within an atmospheric column,

transporting heat, moisture, and momentum, thus changing the properties of all layers affected by convection. In addition, various microphysical processes remove water from and exchange heat with air.

3. COMPARISON WITH GATE OBSERVATIONS

Using this model, local heating and moistening rates attributable to convection are calculated during the tropical Atlantic GATE measurement period. Fig. 2 shows one comparison of calculated and observed heating and moistening rates resulting from convection. During GATE, both the placement and magnitude of the convective-scale heating and moistening are reasonably simulated when the convective mass fluxes and detrainment lengths are forced to produce exactly the observed precipitation rate. Using the model operating in a prognostic mode, GATE measurements can be accurately simulated when convective mass fluxes and detrainment lengths are specified as follows.

Convective mass fluxes: GATE measurements show that during periods of more intense convection, a larger depth of the atmosphere is unstable with respect to turbulent-scale perturbations in heat, moisture, and vertical velocity. This suggests that an approximately constant fraction of the mass of any unstable layer (M_{unstable} kg m⁻²) is lofted per unit time. Using a fairly conservative definition of what constitutes an unstable layer (positive acceleration, $dw/dz > 0$ in Eq. 1, following a small vertical displacement of air 0.7 °C warmer, 0.7 g kg⁻¹ moister than environment) we find that the convective mass flux (M_c) from any layer of the atmosphere can be expressed as:

$$M_c = \frac{M_{\text{unstable}}}{\tau_v} \quad (3)$$

Here τ_v is a "venting" time scale, empirically determined from GATE measurements to be about 35 hours.

"Detrainment lengths": GATE measurements show that during periods when the upper troposphere is relatively dry, convective activity is suppressed, suggesting that buoyant plumes detrain their mass at lower levels, yielding less lifting, condensation, and precipitation. The best agreements between model calculations and observations occurs when

$$l_d(\text{km}) = 15 \exp\left(\frac{Rh-1}{0.4}\right) \quad (4)$$

When the atmosphere is nearly saturated ($Rh=1$), cumulus plumes would rise to 15 km before "shedding" 63% of their initial mass. However, this characteristic depth decreases substantially in drier air.

4. DISCUSSION AND CONCLUSIONS

We have developed a multi-stream model of convection for diagnosing vertical profiles of heat ($\partial T/\partial t$) and moisture ($\partial q_v/\partial t$) tendencies, and precipitation rates attributable to buoyantly-forced motions. Mass fluxes between atmospheric layers are calculated by assuming that buoyantly-accelerated plumes detrain mass as they rise, in contrast to conventional models that treat cumulus clouds as entraining entities. We test this

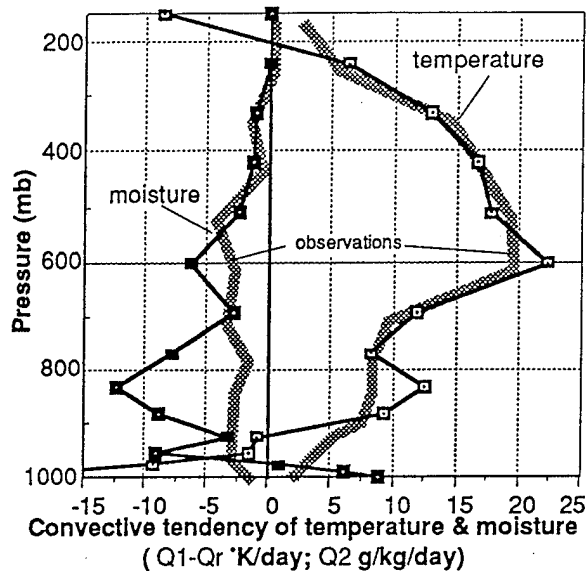


Figure 2. Calculated and observed heating rate ($\partial T/\partial t$ °K day⁻¹) and moisture tendencies ($\partial q_v/\partial t$ g kg⁻¹ day⁻¹) due to convection in the GATE measurement area at 15 UTC, 2 Sept. 1974. Observations are thick gray lines.

parameterization using GATE measurements, and find that periods of heavy convection are associated with deeper unstable layers, suggesting that approximately 2-3 % of the mass within unstable atmospheric layers is "lofted" per hour. In addition, our results suggest that cumulus updrafts more efficiently transport mass vertically in low shear, high humidity environments. Our parameterization includes effects associated with updrafts and downdrafts, cumulus-induced subsidence, and generation and evaporation of precipitation using relatively sophisticated treatment of microphysics. While our model makes no assumptions about larger scale forcings, the calculated heating and moistening rates attributable to convective processes naturally balance the larger-scale destabilization tendencies. This detraining model is conceptually simpler yet more physically representative of actual cumulus ensembles, and may eventually yield more accurate treatment of convection within numerical weather prediction models.

Acknowledgments. The authors are grateful to the NSF, AFOSR, and the DOE for supporting this research. We also gratefully acknowledge J. Wang and D. Randall of CSU for providing processed GATE measurements.

REFERENCES

- Arakawa, A. and Schubert W. 1974. Interaction of cumulus cloud ensembles with the large-scale environment part 1. *J. Atmos. Sci.*, **31**, 674-701.
- Raymond, D. and A. Blyth 1992. Extension of the stochastic mixing model to cumulonimbus clouds. *J. Atmos. Sci.*, **49**, 1968-1983.
- Warner, J., 1970: On steady-state one-dimensional models of cumulus convection. *J. Atmos. Sci.*, **27**, 1035-1040.

Proceedings
of the
**CLOUD IMPACTS ON DOD OPERATIONS
AND SYSTEMS 1993 CONFERENCE**
(CIDOS - 93)

COLOR COMPOSITE



GMS 0336 UTC

VISIBLE = YELLOW
INFRARED = BLUE

SERCAA 0400 UTC



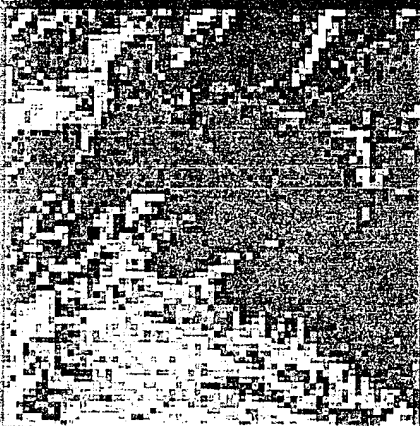
0 100
CLOUD FRACTION

TOPOGRAPHY



0 3.5 7
ELEVATION (KM)

OLS 0319 UTC



0 100
CLOUD FRACTION

AVHRR 0216 UTC



0 100
CLOUD FRACTION

GMS 0336 UTC



0 100
CLOUD FRACTION

16-19 November 1993
U.S. Army Topographic Engineering Center
Fort Belvoir, Virginia

CLOUD COVER AND ITS RELATIONSHIP TO OTHER METEOROLOGICAL FACTORS DURING A SPRINGTIME MIDLATITUDE CYCLONE

Chris J. Walcek
State University of New York, ASRC
Albany, New York, 12205. telephone: (518)442-3840

Abstract

Short-term 3DNEPH cloud observations are compared with standard meteorological measurements during a springtime midlatitude cyclone. Cloud cover is strongly correlated with relative humidity, and appears to decrease exponentially (not linearly) as relative humidity falls below 100%. The middle troposphere contains the highest cloud amounts at the lowest relative humidities (e. g. 30% cloud cover at 50% humidity at 650 mb). Current meteorological forecast models specify cloud amounts less than reported by the 3DNEPH, especially in the middle troposphere, where typically no clouds are allowed at relative humidities below 50 - 80%.

Introduction

At any "point" in the atmosphere, clouds form when the vapor pressure of water exceeds the vapor pressure that would be saturated with respect to liquid water or ice. However, within a large air mass, small-scale fluctuations in temperature and/or water vapor concentration can lead to areas where clouds occur even though the concentration of water averaged over the air mass may not be saturated at the mean air mass temperature. In large-scale numerical models of the atmosphere, meteorological properties are resolved only over relatively large air masses, typically several 10's to 100's of kilometers horizontally and ~1000 m vertically. Partial cloudy conditions frequently occur within air masses of this size, requiring regional or global-scale meteorology models to parameterize the radiative and dynamic effects of these subgrid-scale clouds. In most parameterizations of cloud-scale processes, the heterogeneous (or subgrid-scale) nature of cloudiness is approximated by assuming that a fraction of each grid area is occupied by clouds. This cloud fraction is used to apportion a significantly different cloud "forcing" into a "grid-averaged" forcing within grid areas that contain a mixture of clear and cloudy regions.

Most meteorology and climate models assume that the fractional area of cloud coverage is determined by the grid-averaged relative humidity. However, the functional relationship between relative humidity and cloud cover is largely unknown, since few simultaneous observations of cloud cover and relative humidity are available. All formulations assign a "critical relative humidity" between 50-90% above which partially cloudy conditions can occur. Below this critical humidity, all algorithms specify totally clear skies, and at humidities above the critical humidity, cloud fraction increases by differing functional forms to 100% cloud cover at 100% humidity. The functional form and critical humidities used are typically "tuned" within the context of a larger-scale meteorological or climate model to match observed outgoing longwave radiation or planetary albedo¹. Due to differences between alternate atmospheric models, large differences arise in their assumed

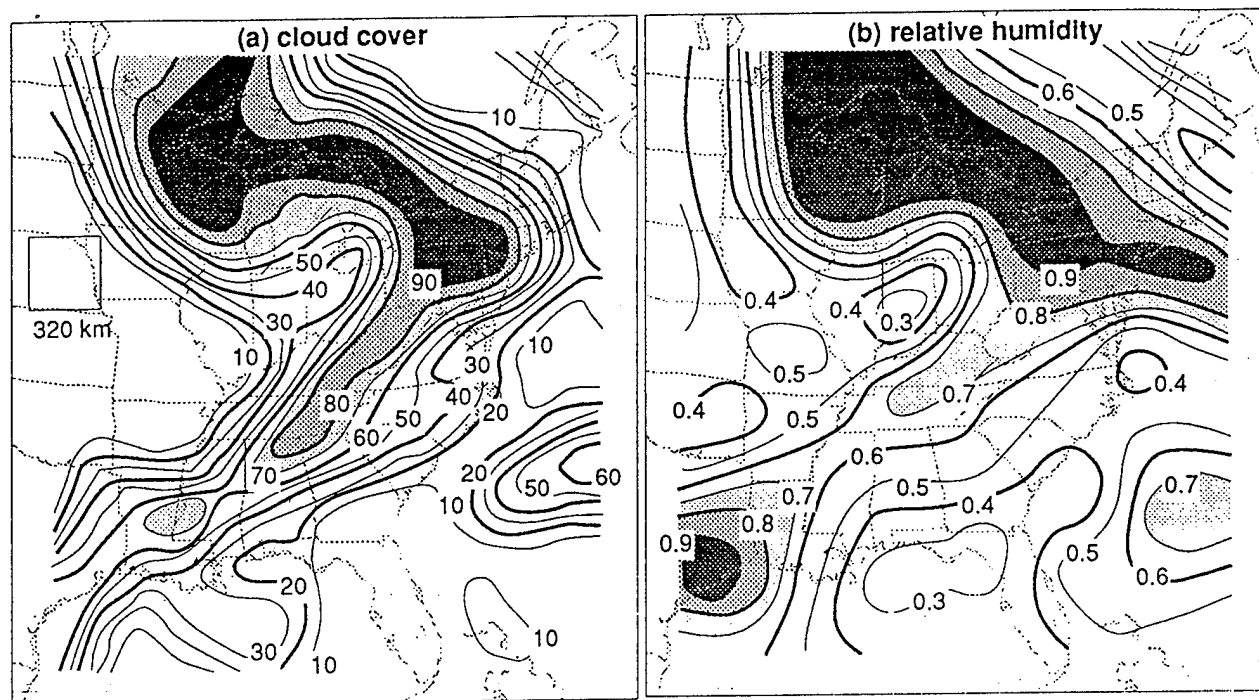


Figure 1: (a) Cloud cover from 3DNEPH cloud archive and (b) Relative humidity dynamically interpolated from upper-air network in the layer 800-730 mb layer at 18 UT, 23 April 1981. Cloud cover and humidity averaged over $(320 \text{ km})^2$ horizontal areas in the layer

relationship between cloud cover and relative humidity. For example, at 800 mb and 80% humidity, the NCAR Community Climate Model² specifies 95% cloud cover (under stable conditions), the British Meteorological Office climate model³ uses 0% cloud cover, while other algorithms^{4,5,6} specify cloud coverage between these extremes.

In this study, we attempt to alleviate the considerable uncertainty in predicting cloud cover by inferring the functional relationship between cloud cover and relative humidity from simultaneous observations of both of these parameters. Previous observational comparisons of cloud cover and relative humidity⁷ are based on limited measurements made under relatively restricted sets of meteorological conditions. For this study, we sample the wide range of meteorological conditions present during the passage of a midlatitude cyclone over the eastern U. S. during spring. Cloud observations are derived from the U. S. Air force 3DNEPH archive, and related meteorological measurements are dynamically interpolated from standard radiosonde measurements using a mesoscale meteorological model.

Cloud cover

The United States Air Force Environmental Technical Applications Center has been receiving and storing Air Force Global Weather Central (AFGWC) cloud data since January 1971. From 1971 to 1983, the AFGWC used an operational real-time three-dimensional analysis of cloud cover referred to as 3DNEPH⁸. The 3DNEPH is a global analysis of cloud cover that uses surface-based and aircraft reports, together with visual and infrared satellite imagery to produce 3-dimensional cloud cover information every 3-hours. Cloud coverage is apportioned into 15 tropospheric levels between the surface and ~16 km above the surface based on routine surface reports of the base and top elevation, and cloud cover in the standard low, middle, and high cloud layers. In areas where surface reports are lacking, satellite imagery and aircraft reports are used to estimate cloud coverage and vertical placement. The data are mapped onto a polar-stereographic global grid from which we have extracted observations over the northeast U. S. for this analysis. Horizontally, the grid size varies from ~25 km near the equator to ~60 km at the poles.

Fig. 1a shows an example of the 3DNEPH-analyzed cloud cover averaged over $\sim(320 \text{ km})^2$ areas in the layer 800-730 mb at local noon, 23 April 1981. A broad region of greater cloud coverage corresponding to a warm frontal region is present over the Great Lakes, and a cold-frontal region extends from Pennsylvania to Texas.

Standard meteorology

Temperature, moisture and dynamical data used in this analysis are taken from observations and spatially and temporally interpolated onto an $(80 \text{ km})^2$ Lambert-conformal grid using a hydrostatic mesoscale meteorology model. Observations are derived from the National Meteorological Center global meteorological analysis and further supplemented using 3-hourly surface observations and 12-hourly radiosonde measurements. Vertically, these meteorological data encompass the surface and 100 mb pressure surface ($\sim 16 \text{ km}$), and horizontally they span the contiguous United States. The vertical grid size of the meteorology data is $\sim 80 \text{ m}$ near the surface, and on the order of a kilometer or more aloft. These observations are provided as initial and boundary conditions to the NCAR mesoscale meteorological model⁹ During model execution, observations are incorporated into the model calculations in regions near observation locations. Differences between observed and calculated temperatures, humidities and wind speeds are continuously minimized through the use of additional tendency terms in the momentum, moisture, and thermodynamic equations which "nudge" the calculation towards the observations. The mesoscale meteorological modeling system is not used to "predict" or "forecast" meteorology. Rather, the model interpolates in space and time several meteorological variables of interest in a dynamically and physically reasonable manner. Thus, model calculations agree closely with observations when and where observations are available, and when no observations are available, the meteorological data are dynamically consistent.

Fig. 1b shows the relative humidity in the 800 - 730 mb layer interpolated from observations using the mesoscale meteorology model described above at the identical time as Fig. 1a. For this figure, temperature and moisture calculations are aggregated into overlapping $(320 \text{ km})^2$ areas, representing a 4×4 average of the 80 km grid used by the MM4. Qualitative comparisons of Fig. 1a and 1b show positive correlations between cloud cover and relative humidity.

Comparison of cloud cover and relative humidity

During the period analyzed, cloud cover maximizes near 900 mb at 35% cloud cover, and decreases to near zero cover at the surface. Above 900 mb, fractional cloudiness gradually decreases to 10-20% cover at 200 mb. As evidenced by comparing Fig. 1a and 1b, cloud cover is positively correlated with relative humidity. We also find weaker positive correlations between cloud cover and large-scale vertical velocity, and negative correlations with wind shear and temperature lapse rate, except in the lowest 100 mb, where cloud cover is weakly correlated with relative humidity, vertical velocity, wind shear and temperature lapse rate. We find that the best single indicator of cloud coverage is relative humidity.

The relationship between cloud cover and relative humidity during this analysis period is assessed by aggregating the observations into increments of relative humidity and cloud cover at each tropospheric level. Fig. 2 shows a joint probability distribution of the 3DNEPH cloud cover and interpolated relative humidity observations in the layer between 800-730 mb, averaged over $(320 \text{ km})^2$ areas. Contours on this figure show the percent probability of observing relative humidity and cloud cover within a particular 5% increment of either of these parameters.

Both cloud cover and relative humidity used in this analysis are highly uncertain quantities to measure. Standard radiosonde humidity measurements are uncertain to $\pm 15\text{-}20\%$, and cloud cover estimates may be uncertain to approximately the same degree. The curve shown on Fig. 2 shows the average cloud cover within each 5% relative humidity increment, and the error bars around this curve show the standard deviation about the mean. Due to the high uncertainty, it is only possible to ascertain the functional relationship between cloud cover and humidity with a large number of samples. The analysis used to generate Fig. 2 has been repeated for all tropospheric levels, and contours of the average cloud cover at various pressures and relative humidities are shown in Fig 3. Cloud cover appears to decrease exponentially as humidity falls below 100%, and relative to other layers in the troposphere, the layers 2.5 to 5 km above the surface contain the highest cloud amounts at the lowest relative humidities, with mean cloud amounts of 30% near 50% humidity at 650 mb.

Based on this analysis, we suggest the following resolution-dependent algorithms for calculating cloud cover (f) from relative humidity (Rh):

$$f(\%) = \min \left[f_{100} \exp \left\{ \frac{Rh - 1}{1 - Rh_e} \right\}, 100 \right] \quad (1)$$

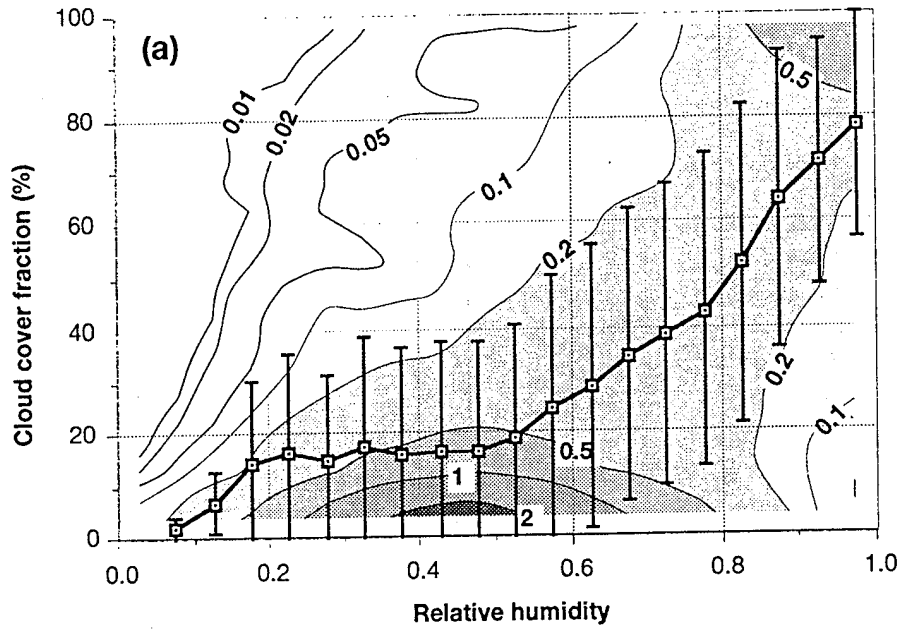


Figure 2: Contours of the probability (%) of observing the cloud cover and relative humidity within a particular 5% increment of each of these parameters. Joint probability distribution for the occurrence of cloud cover at various relative humidities in 800-730 mb layer during 20-24 April 1981. Cloud amounts recorded in the U. S. Air Force 3DNEPH. Relative humidity interpolated from observations using mesoscale meteorology model. Cloud cover and humidity averaged over $(320 \text{ km})^2$ horizontal areas in the layer.

where f_{100} is the cloud cover extrapolated to or at 100% relative humidity, and Rh_e ("e-folding" relative humidity) is qualitatively similar to the "critical humidity" used in previous cloud cover formulations, although here it represents the relative humidity depression below 100% where cloud amount decreases to 37% (e^{-1}) of its value at 100% humidity. The optimum values for Rh_e and f_{100} that produce the minimum difference between observed and calculated cloud cover vary with height in the atmosphere, and are given by

$$f_{100} = f_{\max} \frac{(P/P_s - 0.1)}{0.6}, \quad 0.7 > P/P_s > 0.1. \quad (2a)$$

$$f_{100} = 30 + \frac{(1 - P/P_s)(f_{\max} - 30)}{0.3}, \quad 1 > P/P_s > 0.7. \quad (2b)$$

f_{\max} is the peak value of cloud cover at 100%, which occurs when the atmospheric pressure (P) is about 70% of the surface pressure (P_s), and is weakly dependent on the averaging area (Δx^2) over which cloud cover and relative humidity are calculated over:

$$f_{\max}(\%) = 78 + \frac{\Delta x(\text{km})}{15.5} \quad 80 \text{ km} < \Delta x < 800 \text{ km} \quad (3)$$

The $(1 - Rh_e)$ term in Eq. 1 increases linearly through the depth of the troposphere, and is also influenced slightly by the grid resolution. We suggest the following form:

$$(1 - Rh_e) = 0.196 + \left(0.76 - \frac{\Delta x(\text{km})}{2834} \right) (1 - P/P_s). \quad (4)$$

Using Eqs. (1-4) to calculate cloud coverage from relative humidity, cloud amount can only be assessed to within a root mean square difference of 15 - 30% from the 3DNEPH cloud observations, depending on the resolution at which calculations are performed. This uncertainty is comparable to the uncertainties of the observations.

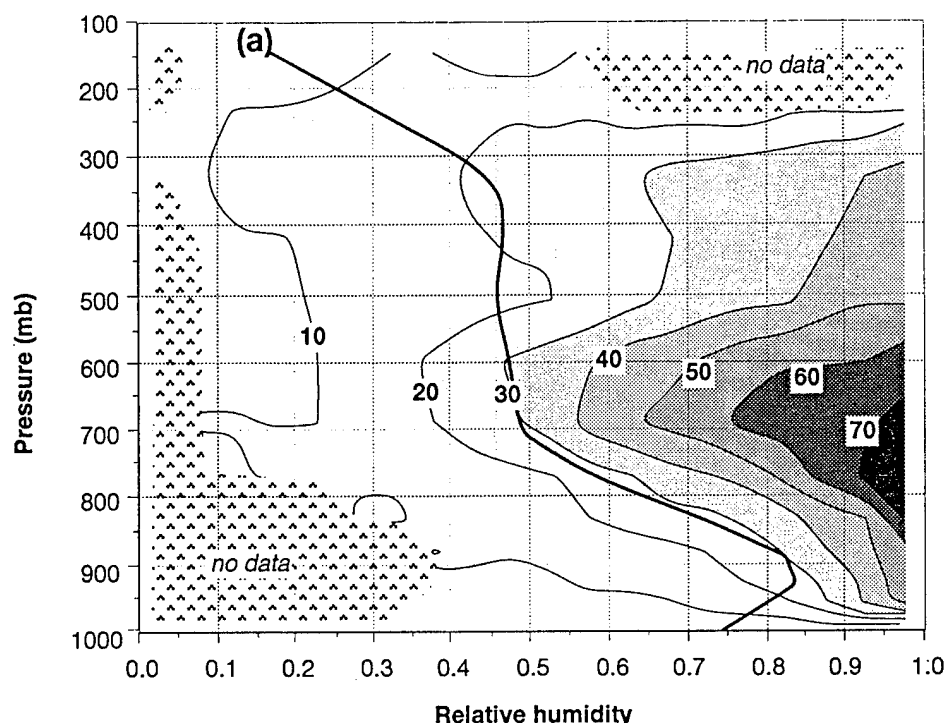


Figure 3: Mean cloud cover (%) at various pressures and relative humidities in the atmosphere during five noon periods during 20-24 April 1981 over the eastern U. S. (domain shown in Fig. 1). Curve shows mean relative humidity during same period.

Conclusions

Vertical distributions of fractional cloud coverage derived from the U. S. Air Force 3DNEPH satellite, aircraft, and surface-based analysis are compared with related standard meteorological observations over the eastern U. S.. Cloud cover and related observations are interpolated onto the identical three-dimensional grid consisting of 15 tropospheric levels at various horizontal resolutions for five local noon periods during a springtime midlatitude cyclone. Mean fractional cloud coverage observed at various relative humidities and pressures are derived from these observations, and resolution-dependent algorithms for estimating cloud coverage from relative humidity are suggested. Despite a high degree of measurement uncertainty, it appears that cloud cover decreases exponentially as humidity falls below 100%, and relative to other layers in the troposphere, the layers 2.5 to 5 km above the surface contain the highest cloud amounts at the lowest relative humidities, with mean cloud amounts of 30% near 50% humidity at 650 mb.

Many meteorological forecast models specify cloud amounts less than reported by these observations. Fig. 4 shows an example of the disagreement between cloud cover calculated by several meteorological models and the trends reported in this study. When relative humidities are less than 90-95% current meteorological models underpredict cloud coverage. This underprediction is especially true in the middle troposphere (850-600 mb), where most algorithms specify zero cloud amounts at relative humidities below 60-80%, while observed cloud amounts (Fig. 3) range from 20-60% at these height and humidity ranges. At humidities close to saturation, current algorithms probably overestimate cloud coverage at many atmospheric levels. The functional relationships between cloud cover and relative humidity proposed in this study are probably more accurate than previous formulations, since they are based on simultaneous observations of both cloud cover and relative humidity.

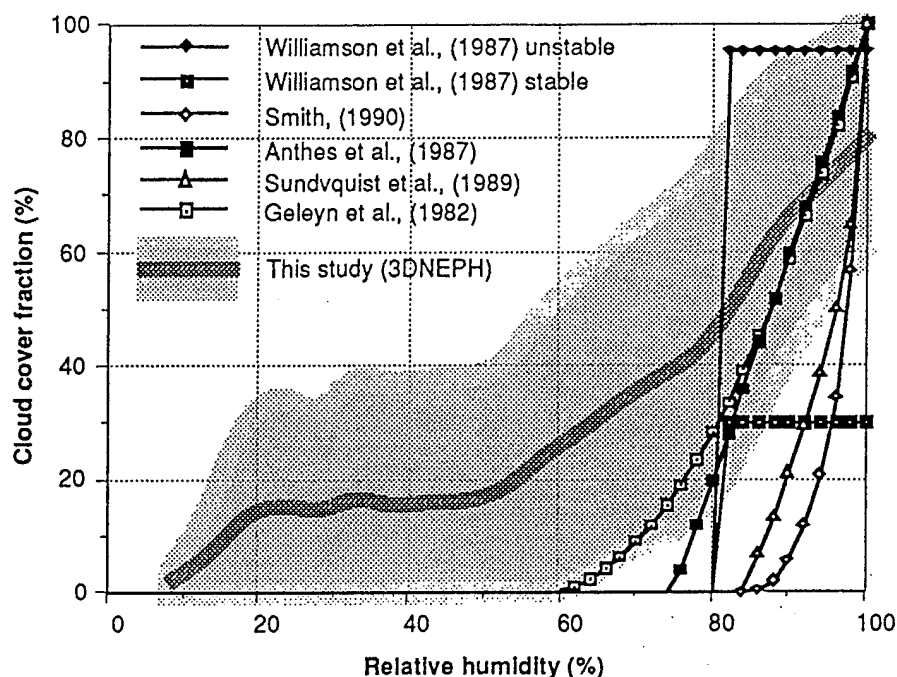


Figure 4: Fractional cloud coverage as a function of relative humidity at 800 mb according to various formulations used by meso- and global-scale atmospheric models. Shaded curve and area shows mean \pm standard deviation of 3DNEPH cloud cover at specified relative humidity during five noon periods during 20-24 April 1981.

ACKNOWLEDGMENTS

The author is grateful to the U. S. Air Force Office of Scientific Research, which is funding this research effort under grant F49620-92-J-0018.

REFERENCES

- ¹Slingo, A. and J. M. Slingo, 1991: Response of the National Center for Atmospheric Research Community Climate model to improvements in the representation of clouds. *J. Geophys. Res.*, **96**, 15341-15357.
- ²Williamson, D. L., J. T. Kiehl, V. Ramanathan, R. E. Dickinson, and J. J. Hack, 1987: Description of the NCAR Community Climate Model (CCM1). NCAR Technical Note NCAR/TN-285+STR, National Center for Atmospheric Research, Boulder, CO 80307.
- ³Smith, R. B. N. 1990: A scheme for predicting layer clouds and their water content in a general circulation model. *Quart. J. Roy. Met. Soc.*, **116**, 435-460.
- ⁴Anthes, R. A., E-Y Hsie and Y.-H. Kuo, 1987: Description of the Penn State/NCAR Mesoscale Model Version 4 (MM4). NCAR Technical note NCAR/TN-282+STR. P. O. Box 3000, Boulder, CO 80307.
- ⁵Sundqvist, H., E. Berge, and J. E. Kristjánsson, 1989: Condensation and cloud parameterizations studies with a mesoscale numerical weather prediction model. *Mon. Wea. Rev.*, **117**, 1641-1657.
- ⁶Geleyn, J.-F., A. Hense and H.-J. Preuss, 1982: A comparison of model-generated radiation fields with satellite measurements. *Beitr. Phys. Atmosph.*, **55**, 253-286.
- ⁷Slingo, J. M., 1980: A cloud parameterization scheme derived from GATE data for use with a numerical model. *Quart. J. Roy. Met. Soc.*, **106**, 747-770.
- ⁸Fye, F. K., 1978: The AFGWC automated cloud atlas model. AFGWC Technical Memorandum 78-002. HQ Air Force Global Weather Central, Offutt AFB, Nebraska 68113, 58 pp.
- ⁹Anthes, R. A. and T. T. Warner, 1978: Development of hydrodynamic models suitable for air pollution and other mesometeorological studies. *Mon. Wea. Rev.*, **106**, 1045-1078.

A CUMULUS PARAMETERIZATION SCHEME OF DETRAINING DRAFTS

Chris J. Walcek and Qi Hu

State University of New York
Albany, New York

1. INTRODUCTION

Most regional- or global-scale models of the atmosphere implicitly ignore cloud-scale vertical motions when they use the hydrostatic assumption to approximate the basic equations of atmospheric motions. This simplification facilitates the simulation of larger-scale atmospheric phenomena. However, under many conditions, nonhydrostatic motions significantly influence larger-scale tropospheric processes, and therefore these "neglected" motions must be accounted for, usually in a simplified or parameterized fashion. In this study, we present a physically-based model of buoyant convective dynamics to describe the effects of clouds on moisture and heat distributions in the atmosphere. Following a description of the model, we evaluate this model using measurements of convection over the tropical Atlantic.

2. CONCEPTUAL MODEL OF CONVECTION

Convective motions are initiated by relatively intense, buoyantly-accelerated updrafts in conditionally unstable areas. As these updrafts mix with the surrounding drier environment, evaporation of cloud-water can induce negatively buoyant downdrafts. Evaporating precipitation can also initiate downdrafts. Subsiding motions in the air surrounding cloudy ensembles will balance any buoyantly-driven fluxes. All of these motions redistribute air within a vertical atmospheric column, and these displaced masses transport heat, moisture, or any other trace constituents from the layer where these motions are initiated to the layers where these motions ultimately stop.

In our model, we assume that buoyantly-accelerated motions are initiated by turbulent impulses within an atmospheric column. In unstable areas, turbulently-"kicked" parcels will accelerate up according to the following equation of buoyant acceleration:

$$\frac{dw}{dz} = \frac{g}{w} \left[\frac{T_{vp} - T_{ve}}{T_{ve}} - q_l \right], \quad (1)$$

where w is the parcel vertical velocity, T_{vp} is the virtual temperature of the rising parcel, T_{ve} is the virtual temperature of the surrounding environment through which the parcel rises, and g is the gravitational acceleration. The condensed water content of the parcel (q_l) is the total water content (assumed constant during lifting) of the parcel minus the saturated vapor mixing

ratio at any level above the lifting condensation level. The temperature and water vapor mixing ratio can be obtained by assuming dry followed by moist adiabatic ascent. As buoyantly-accelerated parcels of air rise, they mix with their surrounding environment. Previous mass-flux models of cumulus convection (e. g., Arakawa and Schubert, 1974) assume that air from outside the cloud is "entrained" into the cumulus updraft, and carried upward. Such a model of entraining plumes may reasonably simulate the behavior of dry plumes. However, in moist plumes where condensation and evaporation are occurring, Warner (1970) demonstrated that such a simplified conceptualization of convective dynamics is inconsistent with observations.

Fig. 1 shows an example of the water content and acceleration of various mixtures formed between air in a moist plume and drier air from outside the plume at two different environmental humidities. Fig. 1 shows that for a moist plume rising and mixing into a relatively moist environment (90% humidity), approximately 50%

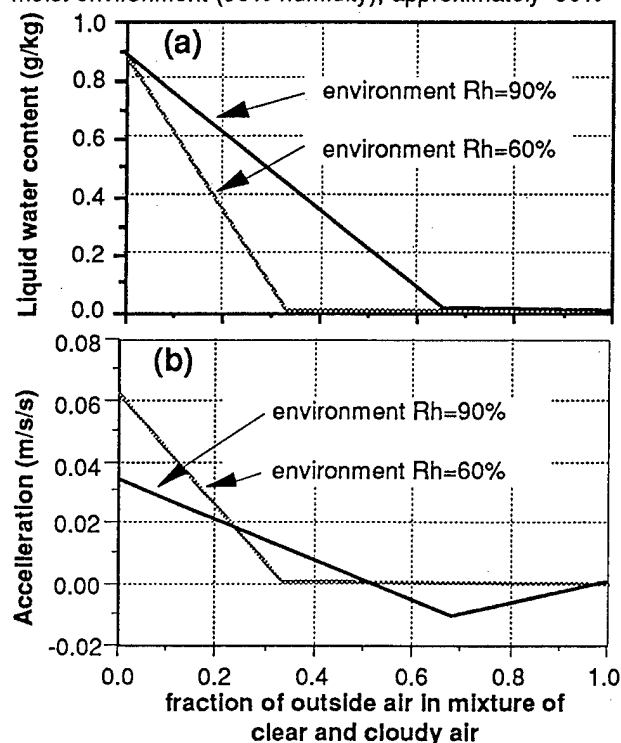


Figure 1. (a) Liquid water content and (b) buoyant acceleration of mixtures of air lifted from 1000 to 900 mb and mixed with varying fractions of air from outside the cloud at 900 mb

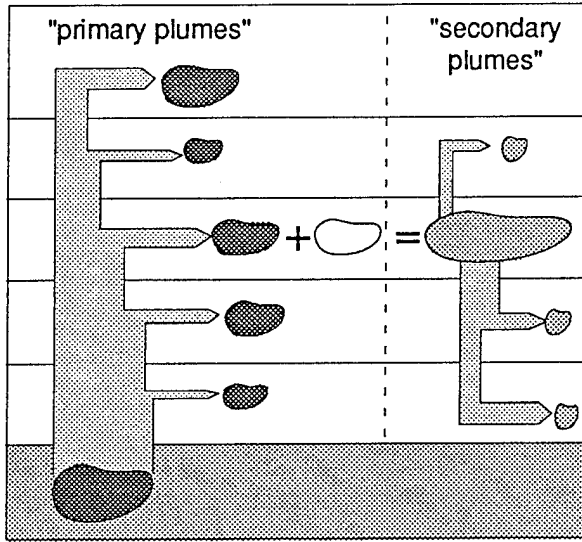


Figure 2. Schematic of the model of convective motions.

of all mixtures that can form are negatively buoyant. As the environment becomes drier, a larger fraction of mixtures that form are negatively or nearly neutrally buoyant. Based on this simple analysis, we propose that moist plumes detrain mass as they rise and mix through a dry environment. Mathematically, this can be expressed as the following equation describing the mass (M) of a rising parcel or plume of air

$$\frac{dM}{dz} = -\frac{M}{l_d} \quad (2)$$

where l_d is a characteristic "detrainment length" that determines the rate of "shedding" of mass from a buoyant plume as it rises. As suggested by Fig. 1, we assume that l_d is locally-defined, determined by the details of how a moist plume interacts with the environment into which it is growing at each level. As shown in Fig. 1, it appears that l_d is shorter (i. e., more detrainment) as the environmental humidity decreases, since less of the mixtures that form are positively buoyant.

Fig. 2 shows schematically the motions considered to be occurring within conditionally unstable environments in our conceptual model of cumulus convection. Air that can accelerate upward under the influence of buoyant forces (as defined using Eq. 1) constitutes what is referred to as the "primary plumes". Air within the primary plumes is "shed" according to Eq. (2). As detrained air at each atmospheric level mixes with its environment, various mixtures will accelerate upward or downward, depending on their buoyancy. We assume that a uniform distribution of mixtures is formed as air is shed from the "primary" updrafts. These mixtures constitute the "secondary plumes" shown in Fig. 2, and these mixtures rise or sink to their level of neutral buoyancy, again shedding mass along the way.

All motions cease as these secondary plumes reach their level of neutral buoyancy.

As air rises in cloudy updrafts, condensed cloudwater can either evaporate or coalesce to form precipitation. We allow cloudwater to evaporate within a characteristic time that depends on the relative humidity of the layer where buoyantly-displaced parcels rise. The formation of precipitation is calculated following Kessler (1969). If a given layer of the atmosphere is near 100% humidity, then cloudwater deposited into that layer will most likely form precipitation. In contrast, in a drier layer, significant amounts of cloudwater can evaporate, and less precipitation forms.

Using Eqs (1-2), together with buoyant acceleration information similar to Fig. 1 calculated for each atmospheric layer, it is possible to calculate the sources and destinations of all buoyantly-induced motions that occur within an unstable column of the atmosphere, and thus construct a "transilient" matrix (Stull, 1988) to describe the local temporal tendencies of heat, moisture, and other trace constituents (C):

$$\begin{bmatrix} C_1^{t+\Delta t} \\ \vdots \\ C_k^{t+\Delta t} \\ C_{km}^{t+\Delta t} \end{bmatrix} = \begin{bmatrix} \delta m_{1,1} & \dots & \delta m_{1,j} & \delta m_{1,km} \\ \vdots & & \vdots & \vdots \\ \delta m_{i,1} & \dots & \delta m_{i,j} & \delta m_{i,km} \\ \delta m_{km,1} & \dots & \delta m_{km,j} & \delta m_{km,km} \end{bmatrix} \begin{bmatrix} C_1^t \\ \vdots \\ C_k^t \\ C_{km}^t \end{bmatrix} \quad (3)$$

The terms of the transilient matrix $\delta m_{i,j}$ denote the fraction of the air arriving at each destination layer j from source layer i , and $\delta m_{i,i}$ is the fraction of air that remains in each layer during the numerical time step Δt . This convective parameterization allows air to move between any possible levels in an atmospheric column, as long as it is dynamically possible for each transition to occur.

Fig. 3 shows graphically the terms of a transilient matrix derived from one period of the GATE measurement program. This transilient matrix represents how air moves under the influence of convection. Initially a tracer for the air at each level is set to a value of 100. Following displacement of a small amount of mass, the final concentration of air at each level is shown in Fig. 3. It is apparent that air from the 1000-900 mb level can be lofted fairly efficiently to the 200-100 mb layer. A bulk of the tracers are displaced a small amount downward due to the forced subsidence of air. Air initially near the 300 mb level subsides downward more than other layers, primarily because this layer was a relatively dry layer, and evaporatively-initiated downdrafts were able to efficiently move air downward about 100 mb at this level.

3. COMPARISON WITH GATE OBSERVATIONS

In order to test the accuracy of our hypothesis of convection, we calculate local heating and moistening rates attributable to convective-scale motions during a period when these tendencies were measured. During August and September 1974, such measurements were

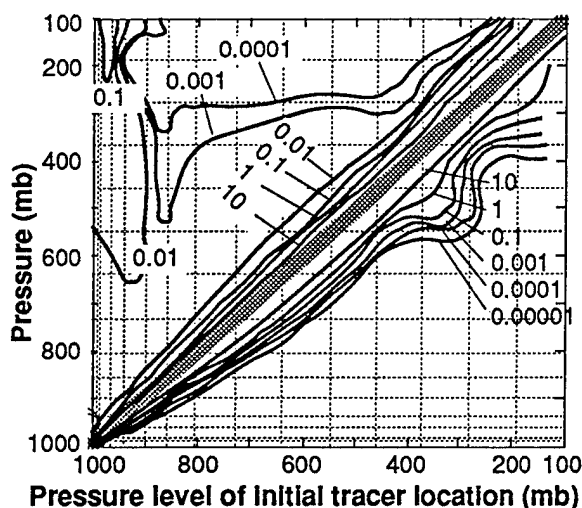


Figure 3. Transilient matrix of the mixing that occurs in the atmospheric column over the GATE measurement region on 2 September, 15 UT. Inert tracer is initially present at concentration of 100, and this pattern represents concentrations at various layers after 14 kg m⁻² have been displaced from those layers that are unstable with respect to small velocity perturbations.

performed as a part of the GATE experiment in the tropical Atlantic Ocean.

Fig. 4 shows one example of the heating rate of the atmosphere resulting from the mixing and rainout prescribed by the transilient matrix shown in fig. 3. For the model calculation, we have diagnostically separated the diabatic effects (condensation and evaporation) from the total effects. For this particular sounding, we find reasonable agreement in both the placement and magnitude of the convective-scale heating. Fig. 5 shows the comparison of the observed and calculated heating rates during the entire GATE observation period for which measurements are available. Except for the second rainy period on 4-5 Sept., the location and magnitude of the convective heating profiles are reasonably reproduced by this conceptual model.

In calculating Figs. 4 & 5, the mixing rates were scaled to exactly reproduce the observed precipitation rate. We are currently assessing a method to calculate the precipitation rate independently. We find that a fraction of the mass of the unstable layer in the atmosphere is lofted per unit time, and this fraction is proportional to the intensity of the convection, as measured by the amount of precipitation produced per kilogram of air lofted. GATE measurements show that during periods when the upper troposphere is relatively dry, convective activity is suppressed, suggesting that buoyant plumes detraining their mass at lower levels, yielding less lifting, condensation, and precipitation. Our analysis suggests that convective heating enhances the convective mass flux, causing a larger fraction of the unstable layer to be lofted per unit time.

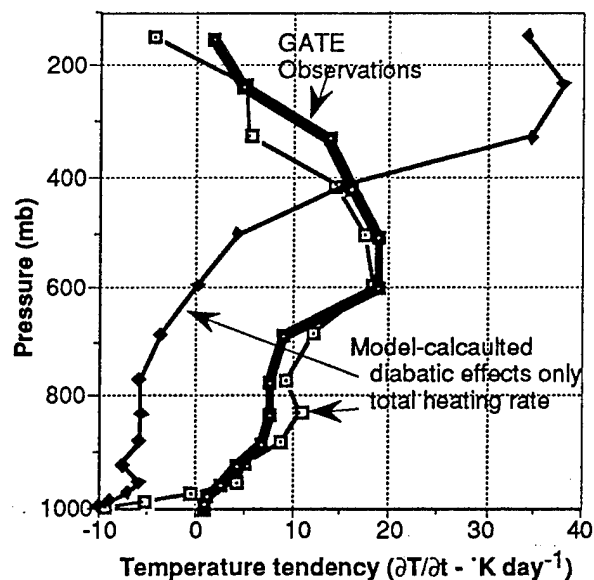


Figure 4. Calculated and observed heating rate ($\partial T/\partial t$ 'K day⁻¹) due to convective-scale processes in the GATE measurement area at 15 UT, 2 September 1974. Observations are local heating rates minus advective and radiative tendencies ($Q_1 - Q_r$).

4. DISCUSSION AND CONCLUSIONS

We have developed a model of cumulus convection to diagnose the heating and moistening rates attributable to cloud-scale motions from the local temperature and humidity profiles within a conditionally unstable atmospheric column. The parameterization is based on a conceptualization that cumulus clouds are composed of turbulently-triggered positively and negatively buoyant parcels accelerating to their level of neutral buoyancy in an atmospheric column, and shedding or detraining mass during transit. When air ultimately reaches its level of neutral buoyancy, it mixes with the surrounding environment, transporting any conserved quantities to the destination level.

The "shedding rate" or detraining length for rising parcels of air appears to be controlled by the local atmospheric relative humidity, with parcels rising to greater heights in high humidity environments. This apparent negative correlation between a "shedding rate" and the environmental relative humidity is consistent with a simple model of turbulent mixing between a moist plume and a dry environment: the drier the environment into which a moist, positively buoyant parcel mixes, the greater the amount of negatively buoyant air that is produced during the mixing process. We have compared heating and moistening rates calculated with this model with measurements from the tropical Atlantic, and find reasonable agreement with the vertical structure and magnitudes of the heating and drying.

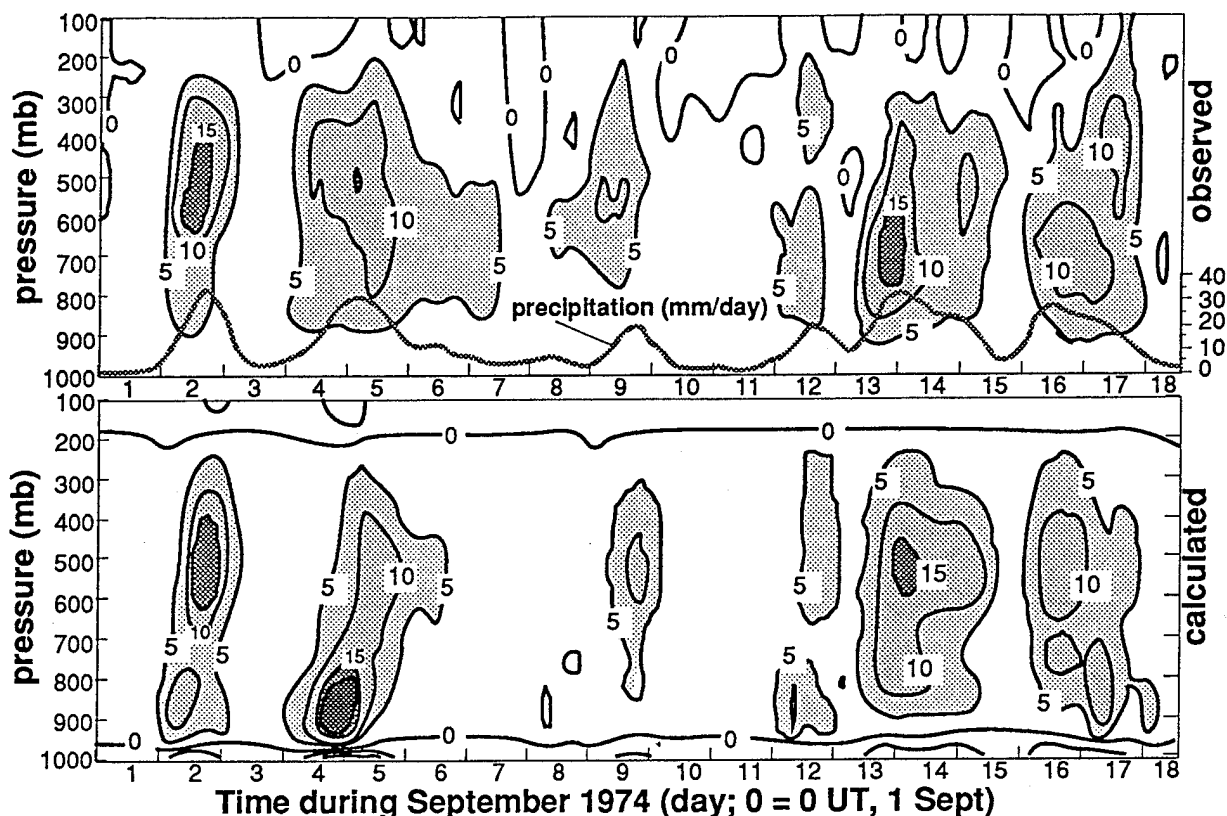


Figure 5. Calculated and observed heating rate ($\partial T / \partial t$ $^{\circ}\text{K day}^{-1}$) due to convective-scale processes in the GATE measurement area during September 1974. Observations are local heating rates minus advective and radiative tendencies ($Q_1 - Q_r$). The top figure shows the observed precipitation rate.

This model of cumulus convection produces results that are consistent with previous parameterizations of cumulus convection, although we make fewer empirical assumptions about the role of larger-scale forcing, and we feel it is based on a more physically accurate concept of cumulus convection. During the GATE observation period, larger-scale destabilization is approximately balanced by the influence of convective-scale processes, a fundamental assumption of the Arakawa-Schubert mass flux scheme. We also find that the atmospheric boundary layer is rapidly dried by convective processes, and thus surface evaporation or larger-scale moisture convergence can often limit the intensity of cumulus convection, an empirical observation upon which moisture-convergence based cumulus parameterizations are based (Kuo, 1974). This convective mixing algorithm can readily be incorporated into existing hydrostatic meteorology models, and is applicable to models of tropospheric chemistry, where details of the mixing process are required to quantify vertical redistribution of trace chemicals in the atmosphere under unstable conditions.

Acknowledgments. The authors are grateful to the U. S. National Science Foundation, the U. S. Air Force Office of Scientific Research, and the U. S. Department of

Energy for supporting the research presented here. We also gratefully acknowledge J. Y. Wang and D. Randall of CSU for kindly providing processed GATE data.

REFERENCES

- Arakawa, A. and Schubert W. 1974. Interaction of cumulus cloud ensembles with the large-scale environment part 1. *J. Atmos. Sci.*, **31**, 674-701.
- Kessler, E. 1969. On the distribution and continuity of water substance in atmospheric calculations. *Meteorological Monographs*, vol 10, #32. American Meteorological Society, Boston, Mass.
- Kuo H. L. 1974. Further studies of the parameterization of the influence of cumulus convection on large-scale flow. *J. Atmos. Sci.*, **31**, 1232-1240.
- Stull, R. B., 1988. Nonlocal closure - transilient turbulence theory, p225-227, in: *An Introduction to boundary layer meteorology*. Kluwer Academic Publishers., Dordrecht, Netherlands, 666 pages.
- Warner, J., 1970: On steady-state one-dimensional models of cumulus convection. *J. Atmos. Sci.*, **27**, 1035-1040.

FACTORS INFLUENCING REGIONAL-SCALE CLOUD COVER: INVESTIGATIONS USING SATELLITE-DERIVED CLOUD COVER AND STANDARD METEOROLOGICAL OBSERVATIONS

Chris J. Walcek

Atmospheric Sciences Research Center
Albany, New York

1. INTRODUCTION

Large-scale numerical models of the atmosphere approximate the heterogeneous, subgrid-scale nature of cloudiness by assuming that a fraction of each grid area is occupied by clouds. This cloud cover fraction is used to apportion cloud effects into a "grid-averaged" forcing within grid areas that contain a mixture of clear and cloudy regions. Most models of tropospheric dynamics assume that the fractional cloud coverage is determined by the grid-averaged relative humidity, stability, or resolvable-scale vertical motions (e. g. Slingo, 1980). In this study, we investigate the relationship between cloud cover and other related meteorological factors by comparing observations of clouds and relative humidity, temperature lapse rates, wind shear, and large-scale vertical velocity within various tropospheric levels.

2. CLOUD COVER OBSERVATIONS

Cloud observations are derived from the United States Air Force operational real-time three-dimensional analysis of cloud cover (3DNEPH). The 3DNEPH is a global analysis of cloud cover that uses surface-based

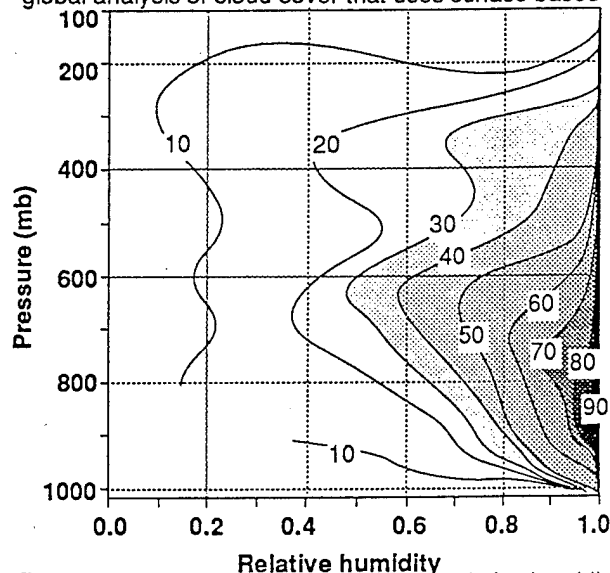


Figure 1. Fractional cloud coverage vs. relative humidity and pressure under stable conditions over the northeast U. S. during 20-24 April 1981.

and aircraft reports, together with visual and infrared satellite imagery to produce 3-D cloud cover information every three hours at 15 vertical layers between the surface and ~16 km above the surface. Horizontally, the grid size varies from ~25 km near the equator to ~60 km at the poles. In this study, we use five noon-time spring periods (20 - 24 April 1981) analyzed over the northeast U. S. by the 3DNEPH. During this five-day period, a relatively intense midlatitude cyclone developed and traversed this domain, allowing one to investigate cloud cover under a wide variety of meteorological environments.

3. RELATED METEOROLOGY

Temperature and moisture observations used in this analysis are taken from the National Meteorological Center global analysis, and spatially and temporally interpolated onto an (80 km)² grid using a hydrostatic mesoscale meteorology model (MM4). During model execution, observations are incorporated into the model calculations in regions near the observation locations. Differences between observed and calculated temperatures, humidities and wind speeds are continuously minimized by "nudging" the calculations towards the observations. In this manner, model calculations agree closely with observations when and where observations are available, and when no observations are available, the meteorological data are dynamically consistent.

4. COMPARISONS

Fig. 1 shows contours of the average 3DNEPH cloud cover at 15 tropospheric levels and at various relative humidities. Typically, 1000 - 5000 (320 km)² observation pairs were available at each layer, and only areas where there is no potential for convection are considered. The cloud observations are averaged within 5% relative humidity increments at each level. As expected, cloud amount increases as humidity increases. At a particular relative humidity, cloud amounts are greatest in the 800 - 600 mb layer, a trend that is consistent with earlier approximations (Buriez et al., 1988). The highest cloud amounts occur under high humidities at 900 - 800 mb, but this figure shows that 10-20% cloud coverage occurs at humidities as low as

15%, in contrast to many formulations, which all set zero cloud cover at humidities below 50 - 80%.

These results suggest that fractional area of cloud coverage decreases exponentially as relative humidity falls below 100%, and that there is no clear "critical relative humidity" where cloud coverage is always zero. We suggest the following approximation for cloud amount f as a function of relative humidity Rh ($Rh < 1$) and vertical velocity w :

$$f = \exp \left\{ \frac{Rh - 1}{\alpha + 0.1 \sigma^2 w} \right\}, \quad (1)$$

where α is a function of height in the troposphere, and represents the relative humidity depression from 100% at which cloud amount falls off to 37% (e^{-1}):

$$\alpha = \begin{cases} 0.2 + \sigma/3 & \sigma < 0.75 \\ 1.8(1 - \sigma) & \sigma \geq 0.75 \end{cases} \quad (2)$$

In Eq. (1) and (2), σ is the pressure relative to surface pressure. Using Eq. (1-2) to calculate cloud cover from Rh and w [averaged over $(320 \text{ km})^2$ areas] produces cloud cover estimates that differ by 10 - 30 percentage points from the 3DNEPH observations.

Based on climate model sensitivity studies, Slingo (1990) estimates that a 15% change in low cloud cover could potentially counter a double- CO_2 warming. If cloud cover changes in response to a change in relative humidity, then there is an important feedback between changing relative humidity and changing cloud cover. Figure 2 shows the present-day global average relative humidity (Rh) according to the NCAR climate model (July conditions). The global-averaged cloud cover calculated using Eq. (1) is also shown on this figure. Error bars on Fig. 2 denote the change in Rh which will induce a 15% change in cloud cover if cloud cover changes with relative humidity as shown in Fig. 1 and approximated by Eq. (1).

5. CONCLUSIONS

We find that a 2-3% increase in relative humidity at 800-900 mb could lead to a 15% increase in cloud cover at these layers. Thus, small changes in relative humidity could counter a CO_2 -induced global warming. These conclusions are based on our comparisons of satellite observations of fractional cloud coverage with co-located related meteorological parameters over the northeast U. S.. We find significant correlations between cloud cover and relative humidity and vertical velocity. These comparisons suggest that cloud coverage decreases exponentially as humidity falls below 100%. Relative to other layers in the troposphere, the middle troposphere contains higher cloud amounts at lower humidities. Most parameterizations of cloud coverage calculate smaller cloud amounts than reported by the 3DNEPH

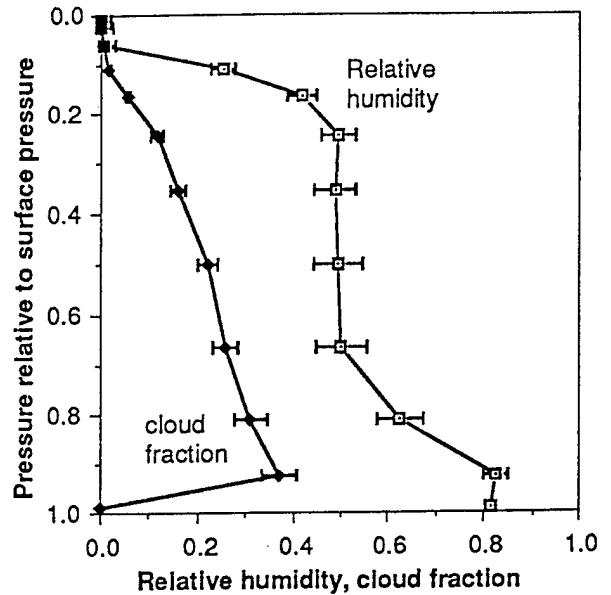


Figure 2. Global average relative humidity and cloud cover according to NCAR CCM1. Error bars denote change in Rh which will induce a 15% change in cloud cover if cloud cover changes with relative humidity as shown in Fig. 1.

observations, especially in the middle troposphere. Furthermore, all cloud cover parameterizations assume that cloud amount is always zero below a "critical" relative humidity, an assumption that is not discernible from this analysis. These results suggest that current methods of calculating cloud cover within large-scale climate simulations or atmospheric chemical modeling studies are significantly underestimating the effects of clouds. More importantly, current climate models probably cannot adequately estimate the potentially significant changes in cloud cover that can result from small changes in relative humidity under dry conditions.

Acknowledgments. The author is grateful to the U. S. National Science Foundation; the U. S. Department of Energy; and the U. S. Air Force Office of Scientific Research for supporting the research presented here.

REFERENCES

- Buriez, J.-C., B. Bonnel, Y. Fouquart, J.-F. Geleyn, and J.-J. Morcrette, 1988: Comparison of model-generated and satellite-derived cloud cover and radiation budget. *J. Geophys. Res.* **93**, 3705-3719.
- Slingo, J. M., 1980: A cloud parameterization scheme derived from GATE data for use with a numerical model. *Quart. J. Roy. Met. Soc.*, **106**, 747-770.
- Slingo, A., 1990: Sensitivity of the earth's radiation budget to changes in low cloud amount. *Nature*, **343**, 49-51.

Cloud cover and its relationship with relative humidity during a springtime midlatitude cyclone: some implications for climate models

Chris J. Walcek

Atmospheric Sciences Research Center
 State University of New York, 100 Fuller Rd., Albany, NY 12205 U. S. A.

1. INTRODUCTION

Microphysical processes occurring within clouds can significantly influence numerous larger-scale dynamic, radiative, and chemical processes occurring in the troposphere (e. g. Walcek et al., 1990). Since clouds are frequently present, it is necessary for accurate models of tropospheric climate or chemistry to account for effects associated with clouds. It is well known that clouds form when the vapor pressure of water exceeds the vapor pressure that would be saturated with respect to liquid water. Within any particular mass of air, fluctuations in temperature or water vapor concentrations can lead to areas where condensation (clouds) can occur even though the water concentration averaged over a larger air mass may not be saturated at the mean air mass temperature.

In large-scale numerical models of the atmosphere, chemical or meteorological properties can only be explicitly resolved over relatively large air masses, typically several hundreds of kilometers horizontally and ~1000 m vertically. It is not unusual to observe significant fluctuations in both temperature and moisture within air masses of this size due to turbulent motions, surface inhomogenities, terrain and other factors, and these perturbations can result in small areas where clouds are present within the grid elements of these larger-scale models. Even though these clouds are not explicitly resolved by many numerical models, their radiative, dynamic, and chemical effects are significant, and their effects must be estimated. Regional or global-scale meteorology models must parameterize turbulent and cloud-scale processes that occur on scales smaller than the model grid size. In most parameterizations of cloud-scale processes, the heterogeneous (or subgrid-scale) nature of cloudiness is approximated by assuming that a fraction (f) of each grid area is occupied by clouds. This cloud cover fraction is used to apportion cloud effects into a "grid-averaged" forcing within grid areas that contain a mixture of clear and cloudy regions.

Most studies of clouds and their effects on tropospheric processes have concluded that even small cloud amounts can exert a significant influence on larger-scale processes. Under these conditions, the net effect of clouds on any physical or chemical process is strongly proportional to f , the fractional area of cloud coverage. Most models of tropospheric dynamics assume that the fractional area of cloud coverage is determined by the grid-averaged relative humidity. More elaborate treatments (Slingo, 1980) allow stability or resolvable-scale vertical motions to influence cloud coverage under some conditions. Figure 1 shows the functional dependence of cloud coverage within a particular atmospheric layer from a survey of formulations currently used by various researchers. All formulations assume a "critical relative humidity" of between 50-90% above which partial cloudy conditions can occur. Below this critical humidity, all formulations assume totally clear skies. At humidities above the critical humidity, cloud fraction

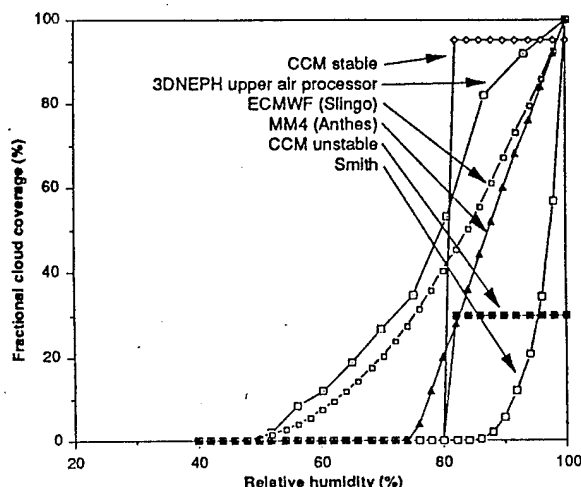


FIG. 1. Fractional cloud coverage as a function of relative humidity at 800 mb according to various formulations used by meso- and global-scale atmospheric models.

increases by some functional dependence to 100% cover at 100% humidity.

Figure 1 shows considerable differences between alternate formulations in assessing cloud coverage within current meteorology and climate models. At 80% humidity, the NCAR Community Climate Model specifies 95% cloud cover (under stable conditions), the British Meteorological Office climate model (Smith 1990) uses 0% cloud cover, while other models specify cloud coverage between these extremes.

In this study, we use observations of both relative humidity and cloud coverage to ascertain the relationship between these two parameters. With a more accurate, observationally-based relationship between cloud cover and relative humidity, the global-scale influence of cloud microphysical processes can be more accurately treated in larger-scale meteorology models.

2. CLOUD COVER OBSERVATIONS

Numerous cloud cover datasets have been collected and analyzed over the past several decades. Hughes (1984) provides a summary of the characteristics of cloud climatologies available in the early 1980's. The earliest cloud climatologies were compiled solely from surface-derived observations, and were often aggregated in time at various latitudes and time of day. Cloud observations in these early datasets were often composed of once-per-day observations averaged over relatively long time frames into seasonal or monthly data at a resolution of 5 - 10° latitude or longitude. Virtually all of the cloud cover datasets reviewed by Hughes (1984) were designed for use in textbooks or climate studies that require relatively coarse temporal and spatial resolutions.

cover within $(320 \text{ km})^2$ stable areas. At a particular relative humidity, cloud amounts are greatest in the 800 - 600 mb layer of the troposphere, a trend that is consistent with earlier approximations (Buriez et al., 1988). The highest cloud amounts occur under high humidities at 900 - 800 mb, but this figure shows that 10-20% cloud coverage occurs at humidities as low as 15%, in contrast to the formulations shown in Fig. 1 which all proscribe zero cloud cover at humidities below 50 - 80%.

These results suggest that fractional area of cloud coverage decreases exponentially as relative humidity falls below 100%, and that there is no clear "critical relative humidity" where cloud coverage is always zero. Based on our analysis of the trends in the average cloud amount shown in Figs. 4 and 5, we suggest the following single-parameter approximation for cloud amount f as a function of relative humidity Rh ($Rh < 1$):

$$f = \exp\left\{\frac{Rh - 1}{\alpha}\right\} \quad (2)$$

where α is a function of height in the troposphere, and represents the relative humidity depression from 100% at which cloud amount falls off to 37% (e^{-1}). Figure 6 shows the value of α in Eq. (2) that yields the minimum root mean square difference between observed cloud amount and cloud amount calculated using Eq. (2). The best fit to the α values shown in Fig. 6 can be reasonably represented by

$$\alpha = 3\left(1 - \frac{P}{P_s}\right) \exp\left\{-3\left(1 - \frac{P}{P_s}\right)\right\} \quad (3)$$

where P is the pressure, and P_s is the surface pressure. Using Eq. (2) to calculate cloud cover from relative humidity [both averaged over $(320 \text{ km})^2$ areas] produced cloud cover estimates that on average contained a root mean square difference of 10 - 30 percentage points from the 3DNEPH observations, depending on which level of the troposphere was being considered.

5. CONCLUSIONS

In this study, we have compared satellite observations

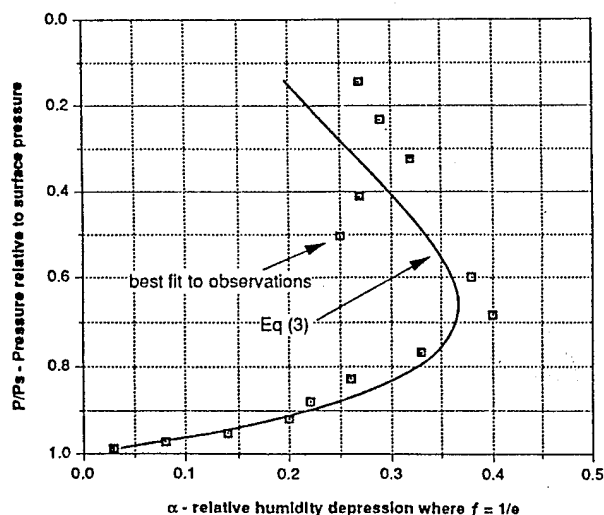


FIG. 6. Vertical variation of the critical relative humidity depression where the average cloud cover is 36.7%. Data points plotted are the values of α in Eq. 2 which yield the minimum RSM difference between 3DNEPH and cloud cover calculated from relative humidity. Curve shows Eq. 3, a reasonable approximation to these data.

of fractional cloud coverage within $\sim(320 \text{ km})^2$ areas with co-located relative humidity observations over the northeast U. S. during a springtime midlatitude cyclone. Cloud cover observations were derived from the U. S. Air Force 3DNEPH analysis of satellite imagery and surface-based observations. Relative humidity was interpolated from observations using a hydrostatic mesoscale meteorology model. Co-located comparisons of the cloud cover and relative humidity and stability suggest that there is considerable uncertainty in any correlations between these parameters over large areas. Despite a high degree of uncertainty, we find significant correlations between cloud cover and relative humidity when data are aggregated into increments of humidity. These comparisons suggest that cloud coverage decreases exponentially as humidity falls below 100%. Relative to other layers in the troposphere, the middle troposphere (700-500 mb) contains higher cloud amounts at lower humidities, with mean cloud amounts of $\sim 30\%$ near 50% humidity.

Most parameterizations of cloud coverage calculate smaller cloud amounts than reported by the 3DNEPH observations, especially in middle tropospheric levels. These results suggest that current methods of calculating cloud coverage within large-scale climate simulations or atmospheric chemical modeling studies are significantly underestimating the effects of clouds. More importantly, current climate models probably cannot adequately estimate the potentially significant changes in cloud cover that can result from small changes in relative humidity.

Acknowledgements. The author is grateful to the organizations that are supporting portions of the research presented here: the U. S. National Science Foundation; the U. S. Department of Energy; and the U. S. Air Force Office of Scientific Research.

REFERENCES

- Anthes, R. A. and T. T. Warner, 1978: Development of hydrodynamic models suitable for air pollution and other mesometeorological studies. *Mon. Wea. Rev.*, **106**, 1045-1078.
- Buriez, J.-C., B. Bonnel, Y. Fouquart, J.-F. Geleyn, and J.-J. Morcrette, 1988: Comparison of model-generated and satellite-derived cloud cover and radiation budget. *J. Geophys. Res.* **93**, 3705-3719.
- Hughes, N. A., 1984: Global cloud climatologies: a historical review. *J. Appl. Clim. and Meteor.*, **23**, 724-751.
- Hughes, N. A. and A. Henderson-Sellers, 1985: Global 3D-neph analysis of total cloud amount: climatology for 1979. *J. Appl. Clim. and Meteor.*, **24**, 669-686.
- Slingo, J. M., 1980: A cloud parameterization scheme derived from GATE data for use with a numerical model. *Quart. J. Roy. Met. Soc.*, **106**, 747-770.
- Smith, R. B. N. 1990: A scheme for predicting layer clouds and their water content in a general circulation model. *Quart. J. Roy. Met. Soc.*, **116**, 435-460.
- Stull, R. B., 1991: Static stability-an update. *Bull. Am. Met. Soc.*, **72**, 1521-1529.
- Walcek, C. J., W. R. Stockwell, and J. S. Chang, 1990: Theoretical estimates of the dynamic, radiative and chemical effects of clouds on tropospheric trace gases. *Atmos. Res.*, **25**, 53-69.